

**AN EXPERIMENTAL STUDY OF THE  
FORMATION PROCESS OF ADIABATIC  
SHEAR BANDS IN A STRUCTURAL STEEL .**

by

**A. Marchand and J. Duffy**  
**Division of Engineering**  
**Brown University**  
**Providence, RI 02912**

**Office of Naval Research**  
**Contract No. ~~N00014-85-K-0597~~**

**Materials Research Laboratory**  
**Grant DMR-8316893**

**April, 1987**

## ABSTRACT

A series of experiments is described in which the local temperature and local strain are measured during the formation of an adiabatic shear band in a low alloy structural steel (HY-100). The specimen employed consists of a short thin-walled tube and the required rapid deformation rates are imposed by loading the specimen in a torsional Kolsky bar (split-Hopkinson bar). The local temperature is determined by measuring the infrared radiation emanating at twelve neighboring points on the specimen's surface, including the shear band area. Indium-antimonide elements are employed for this purpose to give the temperature history during deformation. In addition, high speed photographs are made of a grid pattern deposited on the specimen's surface, thus providing a measure of the strain distribution at various stages during shear band formation. By testing a number of specimens it is possible to form a picture of the developing strain localization process, of the temperature history within the forming shear band, and of the consequent loss in the load capacity of the steel. It appears that plastic deformation follows a three stage process which begins with a homogeneous strain state followed by a generally inhomogeneous strain distribution, and finally by a narrowing of the localization into a fine shear band. It is estimated that the shear band propagates at a speed of about 510 m/s in the material tested. Results also include data on the stress-strain behavior of HY-100 steel over the temperature range -190C to 250C and at quasi-static as well as dynamic strain rates.

## A. Introduction

Numerous studies of shear band formation attest to their importance as a deformation mechanism, e.g. during machining, or perhaps as a failure mechanism during high speed penetration. These studies include extensive experimental observations, modeling of the shear band process, as well as metallurgical studies. Examples can be found in the work of Backman and Finnegan (1973), Rogers and Shastry (1981), and Stelly et al. (1981). Much of this work has been covered in published reviews by Argon (1973), Rogers (1974, 1979), Bedford et al. (1974), Clifton (1980), Olson et al. (1981), Hutchinson (1984), Timothy (1987) on the many different aspects of the subject. Unfortunately, nearly all experimental observations to date are made after the shear band formation process is completed. Only in a few experiments have measurements been made during deformation. Thus, Costin et al. (1979), Duffy (1984) and Hartley and Duffy (1987) attempted to measure the temperature distribution during shear band formation by measuring the infrared radiation emanating at the metal surface, while Giovanola (1987) has taken sequences of photographs with a high speed camera. In the present report both temperature and photographic techniques are employed, but in modified form, to study shear band formation in a structural steel (HY-100). The temperature measurements make use of Hartley's technique, but with an improved optical system. The photographs are taken simultaneously at three locations on the specimen's surface. Three still cameras are used with short duration flash sources rather than a high speed camera, to provide strain measurements at different locations on the path of the shear band. On the basis of the resulting data a picture of the shear band formation process begins to evolve that can be related to predictions made on the basis of the models developed by Molinari and Clifton (1986), Wright and Walter (1987), Dodd and Bai (1985), Freund, Wu and Toullos (1985).

In the experiments described, thin-walled tubular specimens of HY-100 steel are loaded dynamically in a torsional Kolsky (split-Hopkinson) bar at a strain rate of about  $10^3\text{s}^{-1}$  to large enough strains to produce shear banding. Observations of the shear band during its formation is effected by short-exposure photographs of a grid pattern previously deposited on the specimen's surface. As will be seen, the photographs show that plastic deformation goes through three distinct stages. When plastic straining first begins the shear strain distribution is homogeneous and remains so up to a nominal strain of about 25%. In the second stage, strain is inhomogeneous: it varies in a direction parallel to the axis of the specimen. However, in this second stage strain is not a function of the circumferential coordinate. In the final stage, which starts in the neighborhood of 35% to 50% strain, a narrow shear band is seen to form which quickly encircles the specimen. Simultaneously there occurs a sharp drop in the load carrying capacity of the specimen. Subsequent etching with a nital solution reveals white etching bands. In addition to the above, results are also presented of experiments in which the temperature within the shear band is measured during the deformation process. These temperature measurements are effected by employing a set of rapid response infrared detectors to measure the radiation emitted at the specimen's surface. The detectors are calibrated in terms of temperature, and the technique follows the method presented in Hartley et al. (1987) but with an improved optical system.

## **B. Experiments**

### **1. Application of the Torsional Kolsky Bar to Studies of Shear Bands**

The tests described were performed in the torsional Kolsky (split-Hopkinson) bar, shown schematically in Figure 1. The basic apparatus was developed by Kolsky (1949) for compressional loading of wafer-shaped specimens at high strain rates. Baker and Yew (1966), Nicholas (1971), Duffy et al. (1971) modified the apparatus for testing in torsion.

Torsional loading is advantageous for the study of shear bands because there is no change in the cross-sectional area of the specimen during deformation due to necking or barrelling as occurs at high strains in tensile or compressive loading. In addition, the advantage of the Kolsky bar over methods such as impact or expanding cylinder testing is that the average strain rate and the average strain can be controlled easily. However, it must be emphasized that, when interpreting the records, the strain and strain rate are obtained from the relative rotation of the two ends of the specimen. Hence, they represent only average values over the gage length of the specimen and do not provide information about the distribution of the strain or strain rate across the gage section. Thus, when a shear band forms, the strain given by the Kolsky bar records will be an average taken over both the highly strained shear band region and the area outside the shear band. Thus, a local measurement of strain is needed as, for instance, by observations of the deformation of a grid on the metal surface as described in the present paper.

## 2. Description of the Torsional Kolsky Bar

The Kolsky bar used in the present experiments is made of 6061-T6 aluminum alloy 25.4 mm (1.0 in) in diameter and is supported along its length by a series of Teflon bearings. The high strain rates are achieved through the sudden release of a stored-torque at one end of the Kolsky bar, thus initiating a torsional pulse. Electric resistance strain gages measure the magnitude of this stored-torque. Upon release of the torque, a sharp-fronted torsional loading pulse of constant amplitude (equal to half the stored torque) propagates down the bar toward the specimen. Simultaneously, an unloading pulse of equal magnitude propagates from the clamp toward the torque pulley. The mechanical impedance of the pulley is sufficiently large so the unloading pulse, after reflection from the pulley, reduces the torque in the incident bar to zero as it propagates toward the specimen. The duration of the loading pulse at the specimen,

therefore, is the time required for a pulse to travel twice the distance along the bar between clamp and torque pulley. The rise-time of the loading pulse produced with the present apparatus is about 40 microseconds and the duration of the pulse can be varied by changing the position of the clamp along the bar.

Strain gages are mounted on the incident and transmitter bars, the former to measure the incident and reflected pulses and the latter the pulse transmitted through the specimen. Their location along the bars must meet two requirements. First, the gages on the incident bar must be far enough from the specimen to avoid overlap between the incident and reflected pulses. In addition, the gages on the incident and transmitter bars must be mounted at the same distance from the specimen, if the method of Lindholm (1964) is to be used to convert their outputs into a stress-strain diagram for the specimen material. At each station, two four-arm electric resistance strain gage bridges are mounted with the gages sensitive to strain at  $45^\circ$  to the bar's axis. The signals from the gages during testing as well as during calibration are recorded by means of a Nicolet 4-channel digital oscilloscope. As shown by Kolsky, the average strain and stress in the specimen can be inferred, respectively, from the measured records of the strain in the incident and transmitter bar. The reflected pulse provides a measure of the average shear strain rate in the specimen,  $\dot{\gamma}(t)$ , and, through a single integration, provides the average shear strain in the specimen,  $\gamma(t)$ . The magnitude of the pulse transmitted through the specimen is a direct measure of the average shear stress in the specimen,  $\tau(t)$ . Details of these calculations and a more thorough description of the torsional Kolsky bar can be found in Hartley et al. (1985). A schematic diagram of the output from the incident and transmitter bar gages and the oscilloscope output from a typical test are presented in Figure 2.

### 3. Specimen Preparation

The chemical composition of the steel tested, consisting mainly of a tempered martensite microstructure, is given in Table 1. The material is received as bar stock and machined in the shape of a thin-walled tube with integral hexagonal flanges, Figure 3. These flanges fit into matching hexagonal sockets in the Kolsky bars, and their dimensions are such as to provide a torsional impedance equal to that of the aluminum Kolsky bars. Indeed, by means of a separate test it was shown that there is no pulse reflection at the flanges. In addition, to assure no lost motion between sockets and flanges, a set of 12 small set screws in each socket is used to hold the specimen's flanges against the driving faces of the hexagonal sockets. The flanges are chamfered to prevent obstruction of light rays during either photography or temperature measurements.

The specimen proper is the short tube between the two flanges, Figure 3. It has a gage length of 2.5 mm (0.1 in), an internal diameter of 9.5 mm (0.375 in) and a wall thickness of approximately 0.4 mm (0.015 in). The inside and outside walls of the tube are given a fine polish to remove defects due to machining. In the case of short-exposure photographs, this fine polish is followed by a very light etch to dull somewhat the mirror finish and thus improve the quality of the subsequent photographs. To measure the shear strain distribution a grid of fine lines is deposited on the outside surface of the specimen. Initially, these lines are oriented parallel to the axis of the specimen, so that during deformation their slope provides a measure of the strain distribution across the gage section. The grid pattern, consisting of 98 lines per cm (250 lines per inch), is deposited by a photoresist process. It remains visible throughout the deformation process and is recorded photographically during deformation by means of a high speed flash, Figure 4. Examples of such patterns during deformation are shown in Figures 4a, 4b and 4c. In the first instance, Test 11, the lines are inclined but straight, implying homogeneous deformation. In the second, Test 16, the lines are

slightly curved, illustrating an inhomogeneous shear strain distribution. In the third, Test 15, the slope of the lines is not constant and the large inclination indicates a region of high local strain, Figure 4c. By measuring the angle of inclination, a direct measure of the strain distribution along the gage length can be determined. A similar method, employing scribed lines on the inside surface of the specimen, had been employed by Costin et al. (1979) and was used in some of the present tests, Figure 5. In the case of highly localized deformation, such as in a narrow shear band, the intense local displacement leads to a rather large relative displacement of the printed lines on the two sides of the shear band. In order to identify lines correctly on either side of the band, the grid pattern includes a number of broader lines and occasional different spacing. This insures a correct determination of strain.

#### **4. Technique for Taking Short-Exposure Simultaneous Photographs of the Shear Bands**

The schematic diagram in Figure 6 shows the experimental arrangement. Three still cameras are focussed on the specimen to provide simultaneous photographs of the specimen's surface at points  $90^\circ$  apart. The 35 mm single lens reflex cameras are equipped with standard 50 mm focal length lenses and 110 mm extension tubes to give a magnification of about 2.2. They are loaded with 400 ASA black and white film. Each camera is focussed on a specimen area at a working distance of about 50 mm, as measured from the front the lens to the specimen. Focussing is performed with a steady light source.

During testing, light from a high speed flash source is guided to the observed area on the specimen's surface by means of fiber optic tubes. The duration of the flash is less than 2 microseconds. The spark unit is associated with a delay circuit which controls the time at which the flash fires during passage of the loading pulse, and the system is triggered by a set of strain gages mounted on the incident bar. In each experiment, the instant at which the light flashes is detected by a photodiode and

recorded as part of the stress-time oscillograph. Its timing relative to the stress-time curve is easily deduced from the velocity of the torsional pulse in the Kolsky bar. A photograph of the grid is taken before, during and after each test.

The procedure followed for each test is to darken the room, open the camera shutters, trigger the pulse which loads the specimen and fires the flash tubes at the appropriate instant. The shutters are then closed and the film advanced. The aperture employed provides only a fairly short depth of field on the curved surface of the specimen, which implies that care in focussing is of considerable importance. It must be remembered also that the specimen is cylindrical, so that the image recorded on the film is the projection of a cylinder on a plane. As a result, the distance between two successive lines decreases when moving farther away from the center of each photograph. This foreshortening can be taken as negligible in the central portion of the photograph for a length of about 3 mm measured on the specimen. An average magnification therefore can be determined applicable to this area.

For data reduction, two deformed lines are digitized and a mean curve is deduced. The slope  $\alpha(x)$  at any point of this line is a direct measure of the local shear strain  $\gamma(x)$ , defined by  $\gamma(x) = \tan \alpha(x) = \Delta y / \Delta x$ . To increase accuracy in data reduction, measurements of the local shear band width and of the circumferential displacement of the localized deformation are effected by means of a traveling microscope. The local width of strain localization is taken to be the axial distance over which the slope  $\alpha(x)$  remains constant.

## 5. Temperature Measurements

In the present tests, the infrared radiation is detected by means of a twelve-element system constructed by Judson Infrared. It consists of a linear array of twelve individual indium-antimonide (InSb) cells mounted on a Dewar flask cooled with liquid nitrogen to 77°K, Figure 7a. InSb responds to radiation in the 0.5 to 5.5 micron range, which is

adequate for the measurement of shear band temperatures. The detectors are employed in the photo-voltaic mode to give a response time of less than a microsecond, which easily meets present needs. When cooled with liquid nitrogen, the performance of InSb improves by an order of magnitude due to higher responsivity, longer wavelength sensitivity and decreased thermal noise. Each of the elements in the detector array is rectangular with a width of 0.53 mm and a height of 1.80 mm. The separation between the elements on the detector plane is 0.16 mm. The overall length of the detector array is therefore 8.03 mm. By using a linear array of twelve elements, temperature measurements can be effected simultaneously at twelve spots across the specimen gage section, each as a function of time. The output of each element is individually amplified and recorded on one channel of a Nicolet 4-channel digital oscilloscope. A typical record is shown in Figure 8.

### *The Optical System*

The infrared radiation emitted from the specimen's surface was focussed onto the detector by means of a mirror system. Mirrors are required, rather than lenses, required because they avoid the chromatic aberrations due to lens refraction, i.e., the shift of focal length with wavelength. This is particularly important since the infrared detectors respond in a broad range of wavelengths. In addition, a mirror makes it possible to use visible light to focus the system. In previous work, Hartley et al. (1987) employed a single gold plated spherical mirror. A single mirror must be placed off-axis, however, to avoid shading of the radiation by the Kolsky bar and by the specimen. In the present tests, an off-axis system is avoided by employing a reflecting objective of the Cassegrain type, Figure 7b. This optical system, commonly used where high resolution and precision are primary requirements, as for instance in telescopes, employs two confocal paraboloid mirrors. The two mirrors are precisely aligned, and used in such a way that the image formed by each is free of spherical aberration (variation of focus

with aperture). The Cassegrain system is widely used in infrared work requiring good image quality over a very small field, because of the accessibility of its focal point and its relatively low obscuration ratio. Moreover, the Cassegrain system is also diffraction free, so that it imposes no limitation on the smallest resolvable spot width, as does a single mirror. The adjustment of the two mirrors is made to reduce the blur circle at the observed spots, and thus to give the best image sharpness. Consequently, this type of system is applicable only to a single magnification ratio.

In the present tests, a Cassegrain objective from Ealing Electro-Optics with a magnification of 15 and a focal length of 13 mm was employed. This magnification, in view of the detector's dimensions, gives an object spot width of 35  $\mu\text{m}$ , a space between two object spots of 11  $\mu\text{m}$ , and an overall object length on the specimen of 535  $\mu\text{m}$ . The fact that this latter dimension is only about one fifth of the specimen's gage length and that the location of the shear band is uncertain during a test, lead to some unsuccessful tests in which the shear band appears outside the observed area.

Focussing of the detector-mirror system was performed before each test to obtain a sharp image of the specimen's gage section on the element array. For this purpose, the specimen was replaced in the bar by a dummy specimen of precisely the same dimensions but with a small hole (0.44 mm diameter) drilled in the center of its gage section. An 0.05 mm wire was positioned across the hole and a small bulb placed inside the specimen to project the image of the wire onto the element array. Fine adjustments were made by resolving the image of the wire to obtain the best focus on the element array. After focussing was complete, the dummy specimen was replaced by an actual specimen in precisely the same location.

### *Calibration*

Each detector-mirror system was calibrated before and after each series of tests. The first step in the calibration process is to measure the infrared radiation emitted

from an undeformed specimen heated internally. A soldering iron was used for this purpose, while an imbedded thermocouple was used to measure temperature. Temperature and detector output were recorded in increments of 10°C starting at room temperature, heating to the maximum possible temperature and then cooling to room temperature, Figure 9. A rotating notched disk placed between the mirror and the detector was used to produce an AC signal. Each element of the detector was calibrated separately and the response of the twelve elements was found to be almost identical, with the output increasing rapidly at the higher temperatures.

In previous work, Hartley et al. (1987) calibrated the detectors as a function of surface finish. At large strains the surface of the specimen loses its smooth appearance, resulting in a change in emissivity. However, Hartley et al. (1987) found that this change was negligible for temperature greater than about 200°C, which is the range of interest in the present experiments.

## C. Results

### 1. Mechanical Behavior of HY-100 Steel Based on Results Obtained with the Kolsky Bar

Figure 10 gives the room temperature quasi-static and dynamic shear stress-strain curves, as determined by means of the torsional Kolsky bar. Dynamic tests were performed at constant strain rates in the range 300 s<sup>-1</sup> to 5000 s<sup>-1</sup>. The initial static yield stress in shear is about 405 MPa, a value which, after multiplying by  $\sqrt{3}$ , approximates tabulated values of the axial yield stress for this steel. The maximum shear strain at fracture in dynamic loading is about 55%, while it is about 185% in a quasi-static test. The dynamic stress-strain curve follows quite accurately the simple power law

$$\tau/\tau_y = (\gamma/\gamma_y)^n \quad (1)$$

where  $\tau_y$  and  $\gamma_y$  represent, respectively, the values of the initial yield stress and strain,

and where  $n'$  is the hardening exponent. The values of these parameters are given in Table 2. A bilogarithmic plot of stress as a function of strain rate is presented in Figure 11 for different values of the nominal shear strain. From these results, an average rate sensitivity parameter  $m$  of 0.0117 has been deduced, and it appears that this steel is not highly strain rate sensitive in the range of strain rates tested.

The mechanical behavior in shear at different temperatures is given in Figure 12 for a dynamic strain rate of 1000/s, and in Figure 13 for a quasi-static strain rate of  $10^{-4}$ /s. The range of temperatures covered in the various tests is  $-190^{\circ}\text{C}$  to  $250^{\circ}\text{C}$ . These results provide a measure of temperature sensitivity useful in modeling shear band behavior. This parameter is deduced from the slope of a bilogarithmic plot of stress versus temperature and is found equal to -0.33.

At room temperature and for dynamic deformation, the stress-strain behavior, Figure 10, shows a maximum shear stress at about 25% shear strain, followed by a slight decrease in stress with further straining, and finally a rapid drop preceding fracture. The rate at which the stress drops is nearly the same in all tests and appears to be constant through most of the drop. Although the stress values and strain hardening values are reproducible, the nominal strain at which the stress starts to decrease sharply can vary from one test to another over the range 35% to 50%. The maximum deformation reached is 40% in the former case and 55% in the latter. It was found that the light etch used to dull the mirror finish reduces the fracture strain only slightly.

A fine crack always appears in the specimen near the end of the test but, as shown in Figure 2b, frequently occurs before complete passage of the incident pulse. In nearly all cases the crack follows the path of the shear band, the only exception being a few instances when it diverged away just before arrest, Figure 5. After testing, some specimens are broken into two pieces, apparently because the crack traveled completely around the circumference. In others, it travels only partly around the circumference. In

this latter instance, an examination of the unfractured portion reveals the presence of a single rather narrow shear band (in the range 10 to 25  $\mu\text{m}$  wide). Moreover the fracture surfaces show white areas after etching in a nital solution, which is usually interpreted as evidence that a phase transformation occurred during the deformation process, Figure 14. These white etched areas do not cover the full fracture surface. As shown by Giovanola (1987) in tests with a similar loading bar and specimen, there can be a scraping of the two halves of the specimen immediately after fracture. This scraping does not affect the entire surface area, but as shown by Giovanola (1987) the white-etched material covers those surfaces that did not scrape.

The results of tests, presented in Tables 3, 4 and 5, show some variation in the values of maximum stress  $\tau_{\text{MAX}}$ , nominal strain at  $\tau_{\text{MAX}}$ , and particularly maximum nominal strain  $\gamma_{\text{MAX}}$ . These variations follow a general trend: the values of  $\tau_{\text{MAX}}$  and  $\gamma_{\text{MAX}}$  increase with the value of nominal strain at  $\tau_{\text{MAX}}$ . This trend was predicted through a numerical analysis performed by Molinari and Clifton (1986) who examined critical conditions for shear localization by considering the size of an initial imperfection in the specimen. In order to apply their analysis to dynamic torsion experiments, variations of the specimen's wall thickness both along the gage length and around the circumference were measured on a 1018 CRS. Although the wall thickness was found to be quite uniform around the circumference, it varied significantly, from 5% to 10%, along the specimen's length. Thus by considering a sinusoidal defect along the length of the specimen, these investigators were able to predict shear stress-strain curves in good agreement with experimental results both for 1018 CRS and 1020 HRS. Moreover these curves show a decrease in the values of  $\tau_{\text{MAX}}$ ,  $\gamma$  at  $\tau_{\text{MAX}}$  and  $\gamma_{\text{MAX}}$  with an increase of the defect size. It seems likely that, in light of these results, the size of the geometrical defect plays an important role in the variations observed in our present results. However more detailed experimental work, in correlation with a numerical analysis, is needed to relate the influence of the defect size to the variation of the shear

stress-strain curves.

During the sudden drop in stress which occurs near the end of each test, the localized strain can become quite large and changes rapidly from one location to another. Thus, in the case of Test 16, Figure 4b, the photograph was taken after but near the maximum load while the stress was decreasing only slowly. However for Test 15, Figure 4c, the photograph was taken during the sharp decrease in load. The photograph from Test 16, Figure 4b, shows an inhomogeneous strain distribution, while a shear band appears on the photograph from Test 15, Figure 4c. Thus the localized strain is much larger in Test 15 than in Test 16, 1100% as opposed to 70%. For Test 16 straining outside the band continues to increase, leading to a shear band at an average strain of about 36% and to fracture at about 50%. It should be pointed out that the photographs in Tests 15 and 16 are taken at nearly the same value of nominal strain. The fact that localization is much more pronounced in one test is consistent with the earlier drop in stress.

## 2. Simultaneous Photographs at Different Locations on the Path of the Shear Band

Tests were performed to study the strain distribution around the circumference of the specimen at various values of nominal strain. Tables 3 and 4 present the results of all these tests. The average strain rate imposed was 1600/s, Figure 15, and in each test three simultaneous photographs were taken  $90^\circ$  apart. However, the trigger time for the flash,  $t_f$ , was varied from one test to another to cover a range of values of average shear strain in the specimen,  $\gamma_f$ , at which photographs are recorded. Since the duration of the loading pulse was 460  $\mu$ s, the trigger time  $t_f$  was varied from 150  $\mu$ s to 320  $\mu$ s, which corresponds to a variation in the instantaneous average strain  $\gamma_f$  ranging from about 20% to 52%. This range of values for  $\gamma_f$  was chosen, based on the appearance of the dynamic stress-strain curve, to provide information on the initiation and on the growth of localized deformation at various stages in the deformation process.

### 3. Photographic Evidence as to the Process of Strain Localization

The process of strain localization in HY-100 steel is illustrated in the sequence of photographs shown in Figure 16. The nominal strain rate in all five tests was 1600/s and the nominal shear strain values at which the photographs were taken are indicated on the average shear stress-strain curve, Figure 16. Since each photograph requires a different test with a different specimen the results cannot be interpreted with absolute certainty due to differences between tests, particularly due to differences in the value of the maximum strain. However, the photographs do provide considerable information on the initiation and growth of the shear band during the dynamic deformation process.

**Stage I:**  $0 \leq \gamma \leq \gamma_I$ . An examination of the photographs of a number of tests indicates that during the first stage in the deformation process the plastic strain distribution is homogeneous and remains so over the range from initial yield until a strain of about 23% is attained. In this range of strains the three cameras not only show a homogeneous strain at the three locations, Figure 16a, but provide approximately equal values of strain, implying no variation in strain in the circumferential direction. Furthermore, the strain value obtained from the grid pattern also equals the average strain at that instant as determined from the records of the transmitted loading pulse. It also appears that there is a coincidence, or at least that there may be a coincidence, between the value of the strain at peak stress and the end of this first stage in the deformation process.

**Stage II:**  $\gamma_I \leq \gamma \leq \gamma_{II}$ . With continued deformation a second stage is entered in which the strain distribution is inhomogeneous. In HY-100 this occurs after reaching a nominal strain of about 27%, Figure 16b. The results of a number of tests show that in this second stage of deformation the amount and width of the localized deformation are always the same at the three observed points around the specimen, so that in this stage the strain does not seem to be a function of the circumferential dimension. To illustrate these features, Figure 17 presents three simultaneous photographs taken at

three locations on the same specimen, just after the maximum in the shear stress-strain curve ( $\gamma_{\text{AVE}} = 27\%$ ). The average distribution of shear strain along the gage length as determined from the photographs is the same and is given in Figure 18. As deformation proceeds in this second stage there is a continuous increase in the magnitude of the localized strain and a decrease in the width of the region over which localization is occurring. Thus, in the HY-100 steel, with an increase of nominal strain from 27% to 35%, the localized strain increases from about 48% to 170% over a band width that is decreasing from 600  $\mu\text{m}$  to 150  $\mu\text{m}$ . Lastly, one observes that the decrease in the flow stress level is never large within this second stage of deformation.

Figure 16c is one of three simultaneous photographs taken during a test (Test No. 26 in Table 4), just when the stress starts to drop sharply. While the same amount and width of inhomogeneous deformation are displayed in the other two photographs (not shown) as in the lower part of Figure 16c, one can observe that, when moving to the upper part of Figure 16c, the maximum slope of each line increases and the local band width decreases. It seems likely that during this test, a sudden and large increase in localization was initiated near this location, and that the flash was triggered very nearly at the instant of initiation. This sudden increment in the localization of strain constitutes the initiation of what may be termed the true shear band, in the sense not only that localization is much greater than before but also that local strain is known to differ at different locations on the circumference of the specimen. When this increment in localization occurs there may actually be propagation of the shear band in the circumferential direction. The value of the nominal strain when stress first starts to drop defines the end of the second stage of deformation.

**Stage III:**  $\gamma_{\text{II}} \ll \gamma$ . For a nominal strain in this steel greater than about 38%, the flow stress begins to drop rapidly. Photographs taken within this third stage, Figures 16d and 16e, reveal an increase in localization with an increase in nominal strain. Furthermore, a set of simultaneous photographs taken during a test reveal that

the amount and width of the localization have different values at the three separate circumferential points. These differences in strain between the three locations may be large, so that at one point the strain may be nearly homogeneous while at either or both of the other points localization may be pronounced. This is clearly shown in the three photographs displayed in Figure 19. Photograph 2 exhibits inhomogeneous strain across a fairly wide area, with a maximum strain of about 130%. In contrast, the maximum strain in Figures 19a and 19c is respectively about 500% and 1900% and corresponds to localized deformation within a very narrow band. The thin black line along the shear band path of photograph 3, Figure 19c, may indicate the existence of a developing crack; this has not been determined. The shear strain distribution along the gage length as measured from these three photographs is shown in Figure 20. It is evident that the axial position at which the maximum local strain occurs is not the same for all locations, differing perhaps by 100  $\mu\text{m}$ . This indicates that the localized deformation does not lie in a single cross-sectional plane around the specimen. The results also indicate that the strain gradient in this third stage varies considerably as a function of the circumferential dimension.

The photographic evidence indicates quite conclusively that a true shear band, as opposed to a more distributed inhomogeneous deformation, forms simultaneous with the rapid drop in the stress, i.e. forms during the third stage in the deformation process. Although formation of the shear band frequently is followed very quickly by fracture, failure in any accepted sense of the word has already occurred since the specimen has lost its load carrying capacity.

The photographic evidence is not conclusive as to the manner in which the shear band forms: does it nucleate at a number of points at nearly the same instant then join up to form a continuous band around the circumference, or does it nucleate at one site from which it propagates around the specimen? The fact that the shear band does not lie in a single plane would seem to favor multiple nucleation sites. On

the other hand, the very large difference in the magnitude of the localized strain at the different sites, 1900% as opposed to 130% for instance in Test 13, Figure 20, would seem to favor a single nucleation site. As will be seen in the sequel, the evidence from the temperature measurements seems consistent with a single nucleation point. This theory also appears to agree with the fact that the shear band becomes ever narrower as the magnitude of the localized strain increases.

As mentioned previously, an important feature of strain localization is that the shear band becomes narrower as localized deformation increases. This behavior is shown in Figure 21, based on the results of a large number of tests conducted with HY-100. The width,  $w$ , of the shear band can be related to the localized strain,  $\gamma_{\text{LOC}}$ , within the band by a power function of the type

$$\gamma_{\text{LOC}} = a w^b \quad (2)$$

This seems to fit the experimental data quite well when  $a = 125.8$ ,  $b = -0.867$  and for  $w$  expressed in microns. However, the maximum value of the localized deformation at which fracture occurs has not been clearly defined and undoubtedly depends on the particular steel. For HY-100 this value is in the neighborhood of 1500% to 1900% with a corresponding width of about 20  $\mu\text{m}$ . Giovanola (1987) obtained similar results with a 4340 steel which also produces very narrow shear bands of the transformation type. These authors found a maximum local strain at failure of up to 2000% and a corresponding shear band width of 20  $\mu\text{m}$ . Separate tests performed by Marchand and Duffy (1987) with 1018 CRS show similar results, Figure 21. However, it appears that in CRS the shear bands are much wider and that the localized strain is never as great as in HY-100. For instance, the maximum value of the localized deformation before fracture seems to be about 600% with a corresponding width of 100  $\mu\text{m}$ .

A plot of localized deformation as a function of nominal shear strain, Figure 22, indicates that under present test conditions pronounced localization in HY-100 does not occur until an average shear strain of about 38% is reached. Based on observations made after completion of the test and on photographs taken at later stages in the deformation process, it seems that above this value, there is no more straining outside the band and the deformation will keep on increasing inside the shear band. This suggests that the local temperature and the local strain rate rise sharply as the stress collapses. This behavior was predicted numerically by Wright and Walter (1987).

#### 4. Results from Temperature Measurement During Shear Band Formation

Tests were performed to measure the temperature profile during shear band formation. The width of the observed spot on the specimen's surface was 35  $\mu\text{m}$ . In these tests, the average strain rate imposed was about 1400/s, as can be seen from Table 5 which displays the results of the successful tests performed. As mentioned previously, some specimens fractured completely during the test: this is indicated by the letter F in Table 5. In all other specimens a fine crack located within the shear band and going part way around the specimen is visible after completion of the test.

Figure 8 shows the output of two adjacent detectors (No. 8 and No. 9) obtained during Test 13T. A maximum temperature of 460°C was recorded in that test. However, in some tests, the detector outputs exhibit two peaks separated by about 1.54 milliseconds. The first is due to the initial passage of the loading pulse and the second to a reflection of the pulse from the loading pulley. From Table 5, it can be seen that in some tests the detectors did not record a second temperature rise. Presumably, this indicates complete fracture during passage of the initial pulse.

In the present experiments, it should be noted that the width of the observed spot on the specimen (35 microns) exceeded the width of the shear band (20 microns). During

each test, the I-R signals were recorded simultaneously with the incident and transmitter gage outputs. Therefore, the timing of the detector outputs relative to the stress-time curve is easily deduced from the velocity of the torsional pulse in the Kolsky bar. Figure 23 displays the detector outputs recorded during the first loading pulse of Test 13T as a function of time and of axial position. In that test, a shear band formed between detectors 9 and 10 which show the highest outputs on this graph. The corresponding temperature is 460°C for detector 9 and 452°C for detector 10. According to results from short exposure photographs (Section B-2), the strain localizes into a very narrow shear band, reaching a width of 20 μm when the deformation becomes highly localized. Since each spot on the specimen is 35 μm wide and the space between two adjacent spots is 11 μm, the shear band can form either inside a single spot, or else overlap two adjacent spots. In the latter case, two adjacent detectors record almost the same temperature. This was found to occur in most of the successful tests. By considering that the shear band overlaps two adjacent spots  $i$  and  $(i+1)$ , the thermal equilibrium of the spot  $i$  at any time  $t$ , can be written as

$$A_i T_i^4 = A_{hi} T_{hi}^4 + A_{ci} T_{ci}^4 \quad (3)$$

where  $T_i$  is the average absolute temperature measured by the detector over the spot area  $A_i$ ,  $T_{hi}$  is the average temperature over the shear band area  $A_{hi}$  overlapping with the spot area  $A_i$ , and  $T_{ci}$  is the average temperature over the remaining "cold" area  $A_{ci}$  of the spot area  $A_i$ . If we assume that the term  $T_{ci}^4$  is negligible compared either with  $T_i^4$  or  $T_{hi}^4$ , and that the temperature inside the shear band,  $T_B$ , is uniform, so that

$$T_{hi} = T_{h(i+1)} = T_B \quad (4)$$

one can deduce from equation (3) that

$$T_B = \left[ \frac{s}{w-d} (T_i^4 + T_{i+1}^4) \right]^{1/4} \quad (5)$$

where  $s$  is the spot width,  $w$  is the shear band width and  $d$  is the space between two adjacent spots. Estimated values of the temperature  $T_B$  inside the shear band for tests performed with HY-100, are reported in Table 6, which gives an average temperature within the shear band of  $900^\circ\text{C}$ . It is interesting to compare these results with those of similar experiments conducted by Hartley et al. (1987), Marchand and Duffy (1987) to measure the temperature profile during shear band localization in 1018 CRS. In that steel the shear band is much wider than in HY-100, about  $100\ \mu\text{m}$  as compared with  $20\ \mu\text{m}$ . Thus, by measuring the temperature over a spot size of  $35\ \mu\text{m}$ , one should obtain a more accurate value of shear band temperature. Indeed, measurements can be made at more than one spot within the band and these show that the temperature is higher in the center than nearer the edges of the shear band. Thus, the relative width of the shear band and of the observed spot are important. In CRS the wider shear band makes it possible to obtain a more accurate measure of the maximum temperature. For HY-100 with its narrow shear band experiments with a narrower spot (about 7 to  $10\ \mu\text{m}$ ) are needed to measure the temperature.

Similar assessments are deduced through a calculation of plastic work. For 1018 CRS, an average stress value of 410 MPa and a maximum localized strain of 600% lead to a calculated temperature of  $575^\circ\text{C}$ , if 90% of the work is converted to heat. This value is in good agreement with experimental results obtained by Marchand and Duffy (1987). However, for HY-100 the calculated temperature is much higher than the measured temperature,  $1500^\circ\text{C}$  as opposed to  $590^\circ\text{C}$ . As mentioned previously, better experimental results are expected if the observed spot on the specimen can be made narrower than the width of the shear band. Figure 24 shows a graph of temperature versus axial position with respect to the center of the shear band. This graph is obtained by first plotting, for each successful test, the maximum value of the temperature as a function of axial position, and then by taking the estimated position of

the shear band as reference. This graph represents the temperature distribution on each side of the shear band as measured from different tests. An exponential function of the type

$$T = a e^{bx} \quad (6)$$

seems to fit the experimental data quite well for  $a = 543.54$ ,  $b = -0.007$ , and for  $T$  and  $x$  respectively expressed in degrees C and in microns ( $x > 0$ ).

##### 5. Estimation of the Speed of Propagation of the Shear Band in HY-100

If one assumes that a narrow shear band nucleates at one point from which it propagates around the circumference of the specimen, then by plotting temperature history on a stress-time record, it is possible to arrive at an estimated velocity for the propagating shear band. In Figure 25, the temperature history obtained in two different tests is plotted as a function of time along with the simultaneous stress-time record from the output of the gages on the transmitter Kolsky bar. For these two tests, the stress-time records were found to be quite similar. The shape and maximum values of the temperature records displayed in Figure 25 are much the same, except that they occur about 60 microseconds apart. This was found to be the maximum time separating any two temperatures peaks in all tests performed. In Test 13T, the temperature exceeds  $200^{\circ}\text{C}$  just as the stress starts to decrease, and a maximum value of about  $450^{\circ}\text{C}$  is reached during the sharp decrease in the load carrying capacity of the specimen. However in Test 12T, temperature signal occurs later but still during the sharp decrease in stress. Results from short exposure photographs (Section B-2) show that during stage three, i.e. while the load carrying capacity of the specimen is dropping, a very large difference in the magnitude of the localized strain may occur at different sites and the temperature records are consistent with this result, Figure 25. Since the I-R detector is focussed on only one site around the circumference of the specimen, a highly localized

deformation at that site must have occurred earlier in Test 13T than in Test 12T. The 60 microsecond difference in the time between the temperature peaks in these two tests thus may be due to the distance separating the observed spot on the specimen and the circumferential location of the initiation point. Assuming that the shear band nucleates at one site, from which it propagates around the specimen in a single direction, and that it propagates with a constant velocity around the overall circumference in about 60 microseconds, one can deduce that its velocity must be about 510 m/s. However, if the shear band were to propagate in both directions around the specimen, the covered distance would be half the circumference, leading to a velocity of 255 m/s. These results must be viewed as tentative until temperature measurements are made at more than one location on the circumference.

This experimental value of the speed of propagation of the shear band in HY-100 may be compared with the value predicted by Freund, Wu and Toullos (1985). These investigators examined a large block of material containing an imperfection and subjected to deformation in an antiplane shear mode. They considered a nonlinear hyperelastic material for which the constitutive equation reduces to the following in the case of simple shear

$$\tau = \mu_0 k \left[ 1 + \frac{b}{n} k^2 \right]^{n-1} \quad (7)$$

where  $k$  is the amount of strain,  $\mu_0$  is the shear modulus for infinitesimal deformations,  $n$  a hardening parameter and  $b$  a positive constant. This function shows a local maximum in stress,  $\tau_0$ , for  $0 < n < 0.5$ , and for a nominal shear strain  $k_0$  such that

$$k_0 = \sqrt{\frac{n}{(1-2n)b}} \quad (8)$$

Based on a linearization of the governing field equations in the neighborhood of the nominal strain  $k_0$ , the authors derived an equation for the speed of propagation of a shear band  $c$  in the form

$$c = c_0 \left( \frac{2 - 2n}{1 - 2n} \right)^{(n-1)/2} \quad (9)$$

where  $c_0$  is the speed of shear waves in the material. In order to compare the calculated value from equation (9) with the experimental value for HY-100, the material parameters  $b$  and  $n$  were determined at the specific strain level  $k_0$  at which the maximum stress  $\tau_0$  occurs. Since the shear modulus  $\mu_0$  of steel is approximately  $81 \times 10^3$  MPa, and the values of  $k_0$  and  $\tau_0$  for HY-100 are respectively 0.25 and 600 MPa, equations (7) and (8) give the values of  $n$  and  $b$  as respectively 0.4995 and 8000. By inserting into equation (9) the value of the shear wave speed  $c_0$  in steel of 3100 m/s, and the hardening parameter  $n$ , a calculated value of the speed of propagation of a shear band in HY-100 is 550 m/s. Based on present experimental results, the calculated value of the speed of propagation of a shear band in HY-100 is almost exactly the same as the experimental value obtained by assuming that the shear band propagates in a single direction around the specimen.

#### 6. Calculation of the Width of the Shear Band in HY-100

Dodd and Bai (1985) derived an equation for the half-width  $\delta$  of an adiabatic shear band, as a function of the local absolute temperature  $T_*$  and of the local strain rate  $\dot{\gamma}_*$ . This expression may be written as

$$\delta \approx \left( \frac{\lambda T_*}{\tau_* \dot{\gamma}_*} \right)^{1/2} \quad (10)$$

in which  $\tau_*$ , represents the shear stress inside the shear band, and  $\lambda$  is the thermal conductivity of steel, i.e. 54 N/Ks. In order to compare with present results, the local strain rate  $\dot{\gamma}_*$  was estimated from the results of two separate tests in which photographs were taken during the last stage in the formation process of the shear band. The maximum localized deformation measured on the photographs of Test 6 is 850% while it

is 1100% for Test 5, as given by Table 4. The local strain rate  $\dot{\gamma}_*$  can be calculated through the relation

$$\dot{\gamma}_*/\dot{\gamma} = \Delta\gamma_{\text{LOC}}/\Delta\gamma_f \quad (11)$$

in which  $\dot{\gamma}$  represents the nominal strain rate, and  $\Delta\gamma_{\text{LOC}}$  is the increment in local strain corresponding to an increment in the nominal strain  $\Delta\gamma_f$ . Thus, for Tests 5 and 6, Table 4 gives the values of  $\dot{\gamma}$ ,  $\Delta\gamma_{\text{LOC}}$  and  $\Delta\gamma_f$  as, respectively, 1600/s, 250% and 1%. Based on these numbers, an estimated value of the local strain rate  $\dot{\gamma}_*$  is  $4 \times 10^5$ /s, which agrees well with values obtained by Giovanola (1987), who report values in the range  $10^5$ /s to  $10^6$ /s for a 4340 VAR steel. The value taken for the stress  $\tau_*$  is the average of the stress levels at which the photographs were taken in Tests 5 and 6, i.e. 270 MPa. Measurements of the temperature  $T_*$  inside the shear band, Table 5, give a maximum value of  $590^\circ\text{C}$ . By this means a calculated value of the shear band width of 40 microns is obtained. Since two separate tests were needed to calculate the value of the local strain rate  $\dot{\gamma}_*$ , this estimated value can only be considered as approximate. Moreover a more precise measurement of the temperature inside the shear band would undoubtedly lead to a greater value than the one used in this calculation. Thus, although the calculated value of shear band width, based on present results, is only an approximation, the agreement between calculated and experimental values seems quite satisfactory.

#### D. Conclusions

Experiments were conducted to study the formation process of adiabatic shear bands in steel. Thin-walled tubular specimens of HY-100 steel were loaded dynamically in a torsional Kolsky bar. During deformation, local strains and local temperatures were measured separately in two different series of tests. Three still cameras were mounted  $90^\circ$  apart around the specimen to provide three simultaneous short-exposure photographs of a grid pattern on the specimen's surface. These photographs give the

shear strain distribution along the gage length at each location around the specimen. In addition, a twelve-element infrared radiation detector along with a Cassegrain mirror was used to record the temperature history at twelve neighboring points including the shear band. Results show that within a very narrow band (20  $\mu\text{m}$  wide) the local shear strain can reach a value up to 1900%. The maximum recorded temperature rise was 590°C. Etching of the specimen after testing using a nital solution revealed white etching bands.

An examination of the grid patterns photographed during the formation of the adiabatic shear bands reveals that the plastic deformation process of shear localization can be divided into three stages:

1. In the first stage of deformation, i.e., for a nominal shear strain  $\gamma \leq \gamma_I$ , the grid lines printed on the specimen's surface tilt to an angle  $\alpha$  which increases with the imposed strain. However, the lines remain straight,  $\alpha$  is the same at all three locations, and  $\tan\alpha$  is equal to the nominal shear strain as determined from the Kolsky bar records. Thus the shear strain is homogeneous and does not vary as a function of the circumferential coordinate. For HY-100 the value of  $\gamma_I$  is about 25% and seems to coincide approximately with the maximum flow stress in shear.
2. As straining continues, i.e., for  $\gamma_I \leq \gamma \leq \gamma_{II}$ , the grid lines become curved indicating an inhomogeneous shear strain distribution. However, until some nominal strain  $\gamma_{II}$  is attained, curvature of these lines is nearly the same at all locations around the circumference. Thus, the strain distribution though inhomogeneous again is not a function of the circumferential coordinate. While the value of  $\gamma_I$  does not vary much from one test to another, the value of  $\gamma_{II}$  in HY-100 ranges from about 35% to 50%.
3. For strains greater than  $\gamma_{II}$ , the flow stress and hence the load carrying capacity drop sharply. During this rapid drop in stress the strain localizes further into an ever narrower shear band, reaching a width of about 20 microns in HY-100.

The short exposure photographs indicate that very different magnitudes of the localized strain occur at different locations on the circumference. Consistently, results obtained with the I-R radiation technique indicate that local temperature depends strongly on the particular spot observed by the detector. Thus the local strain is a strong function of the circumferential coordinate. The sudden drop in the load carrying capacity of the specimen in this third stage represents catastrophic failure. Eventually, the drop in stress is followed by the appearance of a fine crack located near the center of the shear band. Although, based on present photographs, it is difficult to know at what instant the crack first occurs, it seems that the most likely time is shortly before the flow stress reaches zero. Many of the photographs taken show a crack at one location within the shear band, while at others the specimen appears intact. Indeed, while a number of specimens are completely fractured at the conclusion of the test, in numerous instances the crack has progressed only part way around the specimen. The unfractured region then shows a narrow shear band.

The following explanation can be offered as being consistent with the photographic evidence. In understanding the deformation process, it is important to remember that the stress distribution is approximately homogeneous throughout the specimen even when strain is not. This must hold true until the formation of the narrow shear band when there must be stress concentration near its tip. (The only other time when stress is not homogeneous occurs at the very start of deformation when the pulse first arrives at the specimen, i.e. for low values of strain.) In stage (1), where the strain remains homogeneous, the temperature must begin to rise once plastic straining begins. Calculations show that the temperature rise is about 25°C by the end of this stage of deformation, (although this temperature cannot be measured with the present I-R detectors). This temperature rise lowers the flow stress somewhat from its hypothetical

isothermal level. However, while the strain and stress distributions are homogeneous, or nearly so, the temperature need not be, since the flanges provide heat sinks. Thus the material is somewhat softer nearer the center of the specimen while the stress is nearly constant. This results in, or at least contributes to, a greater deformation nearer the center of the specimen. This process is cumulative, so that the high temperature band becomes progressively narrower, and ever higher strain rates and temperatures are attained in this narrowing band. The entire process easily becomes catastrophic in the presence of a defect whatever its nature (geometric, microstructural, etc.). Thus the formation of an adiabatic shear band is a failure process in its own right, which may or may not ultimately be followed by fracture.

#### ACKNOWLEDGEMENTS

The research support of the Office of Naval Research, Mechanics Division, through contract N00014-85-K-0597, and the NSF Materials Research Laboratory at Brown University, grant DMR 83-16893 is gratefully acknowledged. The authors also wish to thank Mr. G. J. LaBonte for his technical assistance throughout this work.

## REFERENCES

- Argon, A. S., 1973, *The Inhomogeneity of Plastic Deformation*, American Society for Metals, Metals Park, Ohio, Chapter 7, 161.
- Backman and Finnegan, 1973, *Metallurgical Effects at High Strain Rates*, (edited by R. W. Rohde, B. M. Butcher, J. R. Holland, and C. H. Karnes), Plenum Press, New York, 531.
- Baker, W. W. and Yew, C. H., 1966, *J. Appl. Mech.* 33, 917.
- Bedford, A. J., Wingrove, A. L. and Thompson, K. R. L., 1974, *J. Aust. Inst. Metals* 19, 61.
- Clifton, R. J., 1980, Chapter 8, *Material Response to Ultra High Loading Rates*, National Materials Advisory Board Committee, Rep. No. NMAB-356, 129.
- Costin, L. S., Crisman, E. E., Hawley, R. H. and Duffy, J., 1979, *2nd Conference on the Mechanical Properties of Materials at High Rates of Strain*, (edited by J. Harding), The Institute of Physics, London, 90.
- Dodd, B. and Bai, Y., 1985, *Mat. Sci. Tech.* 1, 38.
- Duffy, J., Campbell, J. D. and Hawley, R. H., 1971, *J. Appl. Mech.* 38, 83.
- Duffy, J., 1984, *Mechanics of Material Behavior, The Daniel C. Drucker Anniversary Volume*, (edited by G. J. Dvorak and R. T. Shield), Elsevier, 75.
- Freund, L. B., Wu, F. H. and Toullos, M., 1985, *Proceedings of the Considere Memorial Symposium*, Presse de l'Ecole Nationale des Ponts et Chaussees, p. 125, Paris, France.
- Giovanola, J., 1987, *Proceedings on Impact Loading and Dynamic Behavior of Materials*, Bremen, Federal Republic of Germany.
- Hartley, K. A., Duffy, J. and Hawley, R. H., 1985, *Metals Handbook*, Vol. 8, American Society for Metals, 2168.
- Hartley, K. A. and Duffy, J., 1987, to be published in *J. Mech. Phys. Solids*.
- Hutchinson, J. W., 1984, *Scripta Met.* 18, No. 5.
- Kolsky, H., 1949, *Proc. Phys. Soc., London*, V62-B, 676.
- Lindholm, U. S., 1964, *J. Mech. Phys. Solids*, 12, 317.
- Marchand, A. and Duffy, J., 1987, Brown University Report in preparation.
- Molinari, A. and Clifton, R. J., 1986, Brown University Report No. DAAG29-85-K-0003.
- Nicholas, T., 1971, *Exp. Mech.* 11, No. 8, 370.

Olson, G., Mescal, J. F. and Azrin, M., 1981, *Shock Waves and High-Strain-Rate Phenomena in Metals*, (edited by M. A. Meyers and L. E. Murr), Plenum Press, New York, Chapter 14, 221.

Rogers, H. C., 1974, Drexel University Report, U.S. Army Research Office.

Rogers, H. C., 1979, *Annual Reviews in Materials Science* 9, 283.

Rogers, H. C. and Shastry, C. V., 1981, *Shock Waves and High-Strain Rate Phenomena in Metals*, (edited by M. A. Meyers and L. E. Murr), Plenum Press, New York, Chapter 18, 285.

Stelly, M., Legrand, J. and Dormeval, R., 1981, *Shock Waves and High-Strain-Rate Phenomena in Metals*, (edited by M. A. Meyers and L. E. Murr), Plenum Press, New York, 113.

Timothy, S. P., 1987, *Acta. Metall.* 35, 301.

Wright, T. W. and Walter, J. W., 1987, to be published in *J. of Mech. Phys. Solids*.

## FIGURE CAPTIONS

- Figure 1: Schematic of the torsional Kolsky bar.
- Figure 2: Gage output from torsional Kolsky bar. (a) Schematic diagram showing output of incident and transmitter gages. (b) Oscillograph from a typical test (Test 13T).
- Figure 3: Details of torsional specimen with hexagonal mounting flanges. All dimensions are in millimeters.
- Figure 4: Photographs of the grid patterns obtained in three separate tests at a nominal strain rate of 1600/s and illustrating (a) a homogeneous deformation, (b) an inhomogeneous shear strain distribution, and (c) a shear band.
- Figure 5: Photograph of a specimen surface after testing showing a shear band and a partial fracture. In this test the nominal strain rate is 1600/s. Within the shear band  $\gamma_{\text{LOC}} = 500\%$ .
- Figure 6: Experimental arrangement for taking short-exposure simultaneous photographs of the shear bands.
- Figure 7: (a) Photograph of InSb detector-mirror system showing I-R detector, Cassegrain mirror and Kolsky bar. Distances are not those used for an actual test. (b) Schematic diagram showing Cassegrain mirror.
- Figure 8: Typical output of two temperature detectors. (Test 13T)
- Figure 9: Calibration curve for a spot width of 35 microns.
- Figure 10: Quasi-static and dynamic stress-strain behavior in shear at room temperature. Fracture in the quasi-static loading occurs at a shear strain of 185%.
- Figure 11: Results of quasi-static and dynamic tests. Shear stress as a function of strain rate for various values of nominal strain.
- Figure 12: Stress-strain behavior in shear at a nominal strain rate of 1000/s for six different test temperatures.
- Figure 13: Stress-strain behavior in shear at a nominal strain rate of  $10^{-4}$ /s for four different test temperatures.
- Figure 14: Photograph of the fractured surface of a specimen following dynamic deformation. The surface has been etched with a nital solution resulting in white etched areas.
- Figure 15: A typical stress-strain curve showing the strain values at which the photographs in Figure 16 are taken.

- Figure 16: Photographs of the grid patterns obtained in five separate tests at the nominal strain values shown in Figure 15. The nominal strain rate is 1600/s in each test. Each square in the grid pattern measures 100 microns on a side prior to deformation.
- Figure 17: Simultaneous photographs taken at three locations on the same specimen at a nominal strain of 27%, just after the maximum in the stress-strain curve. Note that the localized deformation is the same at all locations, namely  $\gamma_{\text{LOC}} = 55\%$ . (Test 14 nominal strain rate  $\dot{\gamma} = 1600/\text{s}$ ).
- Figure 18: The shear strain distribution at a nominal strain of 27% as obtained from the three photographs in Figure 17.
- Figure 19: Simultaneous photographs taken at three locations on the same specimen at a nominal strain of 35%. The maximum in the stress-strain curve occurs at a nominal strain  $\gamma = 21\%$ . Note that the localized deformation is not the same at all locations, as shown in Figure 21. (Test 13, nominal strain rate  $\dot{\gamma} = 1600/\text{s}$ ).
- Figure 20: The shear strain distribution at three separate locations on the circumference of the specimen as measured from the simultaneous photographs shown in Figure 19.
- Figure 21: The maximum localized strain as a function of the shear band width in the HY-100 steel and in a 1018 cold-rolled steel. The points represent the results of a number of different tests.
- Figure 22: The maximum localized strain as a function of the nominal shear strain.
- Figure 23: The output of the I-R detectors as a function of time and of axial position in Test 13T. Each spot on the specimen is 35 microns wide and the space between two adjacent spots is 11 microns.
- Figure 24: Measured values of the temperature as a function of axial position with respect to the center of the shear band. Note that the width of the observed spot on the specimen (35 microns) exceeds the width of the shear band (20 microns).
- Figure 25: Typical stress-time curve showing the temperature as a function of time in two separate tests. Note that the peak temperatures are separated by about 60 microseconds.

TABLE 1: CHEMICAL COMPOSITION (WEIGHT %) OF HY 100 STEEL

C	Si	S	Mn	P	Ni	Cr	Mo	Cu	Ti	Va
0.18	0.20	0.005	0.25	0.003	2.51	1.63	0.43	0.037	0.001	0.005

TABLE 2: MECHANICAL PARAMETERS FOR HY 100 DERIVED FROM A POWER LAW FUNCTION (EQN. (1))

Shear Strain Rate $\dot{\gamma}$ ( $s^{-1}$ )	Yield Stress $\tau_y$ (MPa)	Yield Strain $\gamma_y$ Corresponding to $\tau_y$	Hardening Exponent n	Range of Applicability
$10^{-4}$	405	0.012	0.080	$0.02 \leq \gamma \leq 0.20$
3300	463	0.012	0.107	$0.05 \leq \gamma \leq 0.20$

TABLE 3: RESULTS OF TESTS PERFORMED WITH  
HY100 STEEL: DATA FOR STAGES 1 and 2

Test No.	Nom. $\dot{\gamma}$ s <sup>-1</sup>	$\tau_{\max}$ MPa	Nom. $\gamma$ $\tau_{\max}$ %	$\gamma_{\max}$ %	Data on Flash			Photos 1, 2, & 3	
					$t_f$ $\mu_s$	$\gamma_f$ %	$\tau_f$ MPa	w $\mu m$	$\gamma_{loc}$ %
					20	1660	581	31	58
11	1620	597	28	54	187	28	597	2500	28
12	1580	597	25	45	186	27	591	600	48
14	1500	557	22	43	204	27	539	500	55
16	1610	567	23	45	202	31	546	350	70
4	1550	567	23	45	216	33	550	420	65
23	1550	590	29	50	239	36	584	220	85
25	1540	601	31	57	272	40	599	400	70

TABLE 4: RESULTS OF TESTS PERFORMED WITH HY100 STEEL:  
DATA FOR STAGE 3

Test No.	$\dot{\gamma}$ s <sup>-1</sup>	$\tau_{max}$ MPa	$\gamma$ at $\tau_{max}$ %	$\gamma_{max}$ %	Data on Flash			Localized Deformation in Stage 3		
					$t_f$ $\mu$ s	$\gamma_f$ %	$\tau_f$ MPa	Photo No.	w $\mu$ m	$\gamma_{Loc}$ %
13	1710	568	21	38	219	35	185	1	50	500
								2	280	130
								3	15	1900
10	1690	585	24	43	233	37	390	1	25	800
								2	35	550
								3	55	400
8	1600	558	26	48	238	38	505	1	240	140
								2	120	200
								3	40 <sup>to</sup>	500
6	1640	527	23	47	252	41	345	1	25	800
								2	20	850
								3	30	700
5	1580	539	23	41	266	42	200	1	90	280
								2	20	1100
								3	30	920
26	1630	597	31	60	292	47	565	1	100	170
								2	30 <sup>to</sup>	600
								3	100	170
								3	100	200

TABLE 5: RESULTS OF TESTS PERFORMED FOR TEMPERATURE MEASUREMENT WITH HY100 STEEL AND WITH A SPOT SIZE OF 35  $\mu\text{m}$

Test No.	Nom. $\dot{\gamma}$ $\text{s}^{-1}$	$\tau_{\text{max}}$ MPa	Nom. $\gamma$ at $\tau_{\text{max}}$ %	$\gamma_{\text{max}}$ %	Shear Band Fracture	Max $\Delta T$ ( $^{\circ}\text{C}$ )	
						1st Load	2nd Load
1T	1280	623	26.4	47	SB	595	746
3T	1360	629	24.9	46	SB,F	465	0
5T	1320	615	23.0	45	SB,F	519	0
7T	1350	606	27.4	52	SB	425	405
8T	1430	613	23.4	47	SB,F	455	0
12T	1330	622	27.2	51	SB	450	316
13T	1290	625	24.3	50	SB	460	332
15T	1420	619	33.5	63	SB	428	652

Table 6: ESTIMATED MAXIMUM TEMPERATURE IN SHEAR BAND  
of HY-100 (EQUATION 5)

Test. No.		1T	7T	8T	12T	13T
Measured Values	$T_i(^{\circ}\text{C})$	566	415	410	450	460
	$T_{i+1} (^{\circ}\text{C})$	590	425	455	424	452
Estimated Values	$T_B(^{\circ}\text{C})$	1140	875	900	900	935

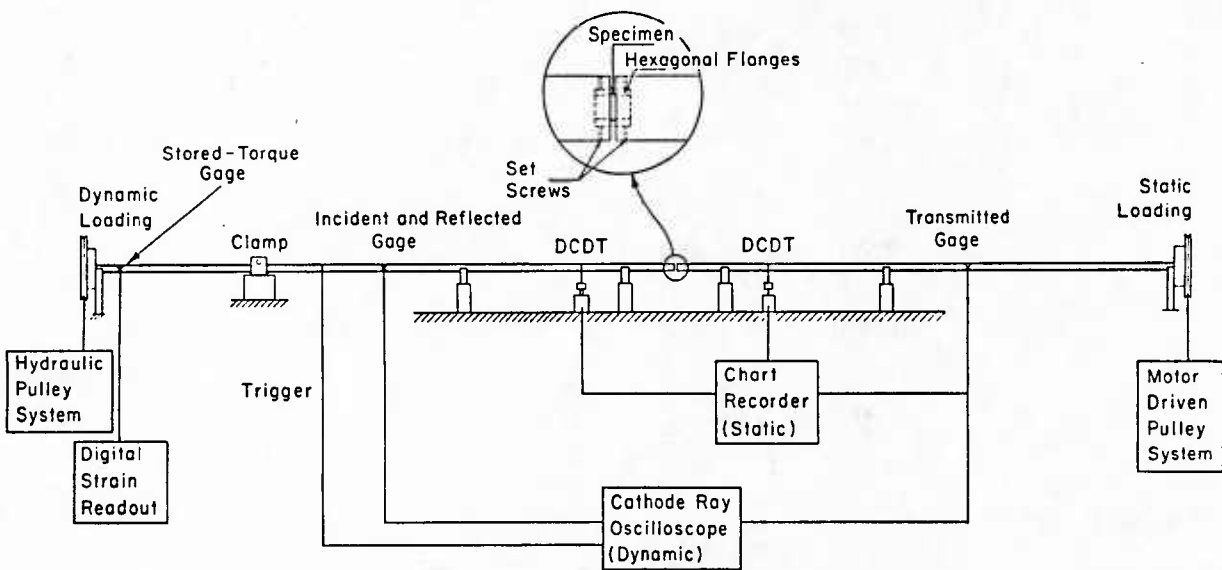


Figure 1: Schematic of the torsional Kolsky bar.

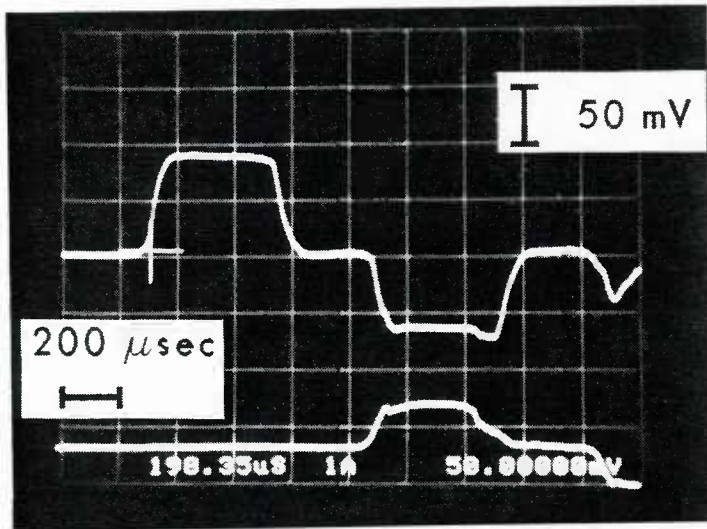


Figure 2: Gage output from torsional Kolsky bar. (a) Schematic diagram showing output of incident and transmitter gages. (b) Oscilloscope from a typical test (Test 13T).

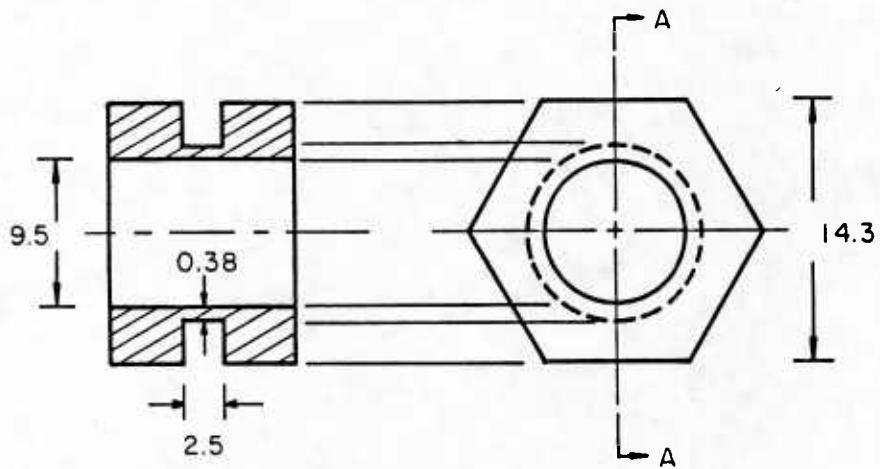
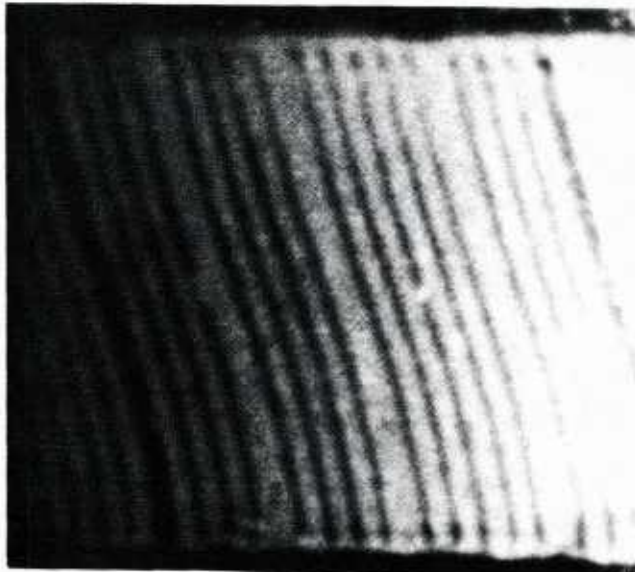


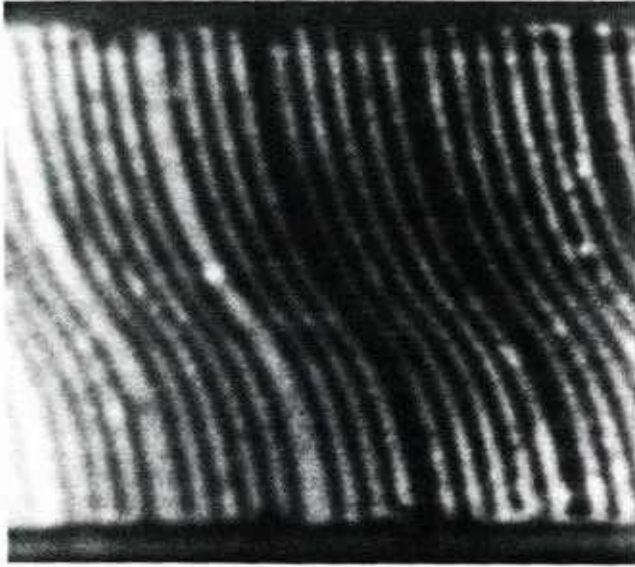
Figure 3: Details of torsional specimen with hexagonal mounting flanges. All dimensions are in millimeters.

**HY-100 Steel**



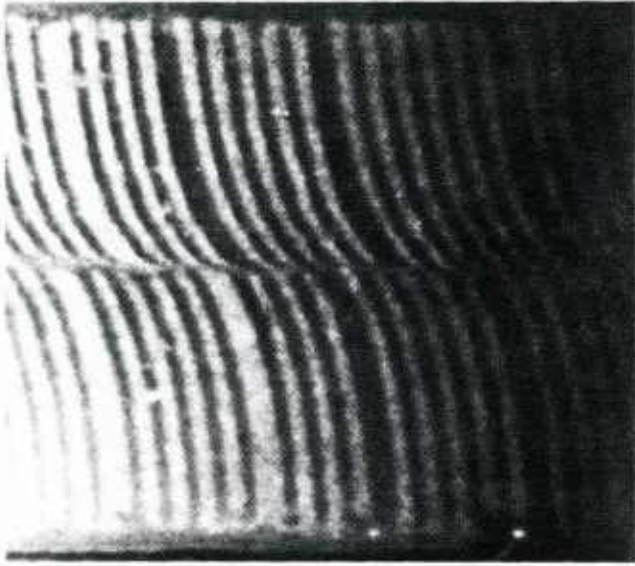
**Test 11**

**Homogeneous  
Deformation**



**Test 16**

**Inhomogeneous  
Deformation**



**Test 15**

**Shear  
Band**

**Figure 4:** Photographs of the grid patterns obtained in three separate tests at a nominal strain rate of 1600/s and illustrating (a) a homogeneous deformation, (b) an inhomogeneous shear strain distribution, and (c) a shear band.

**0.5 mm**

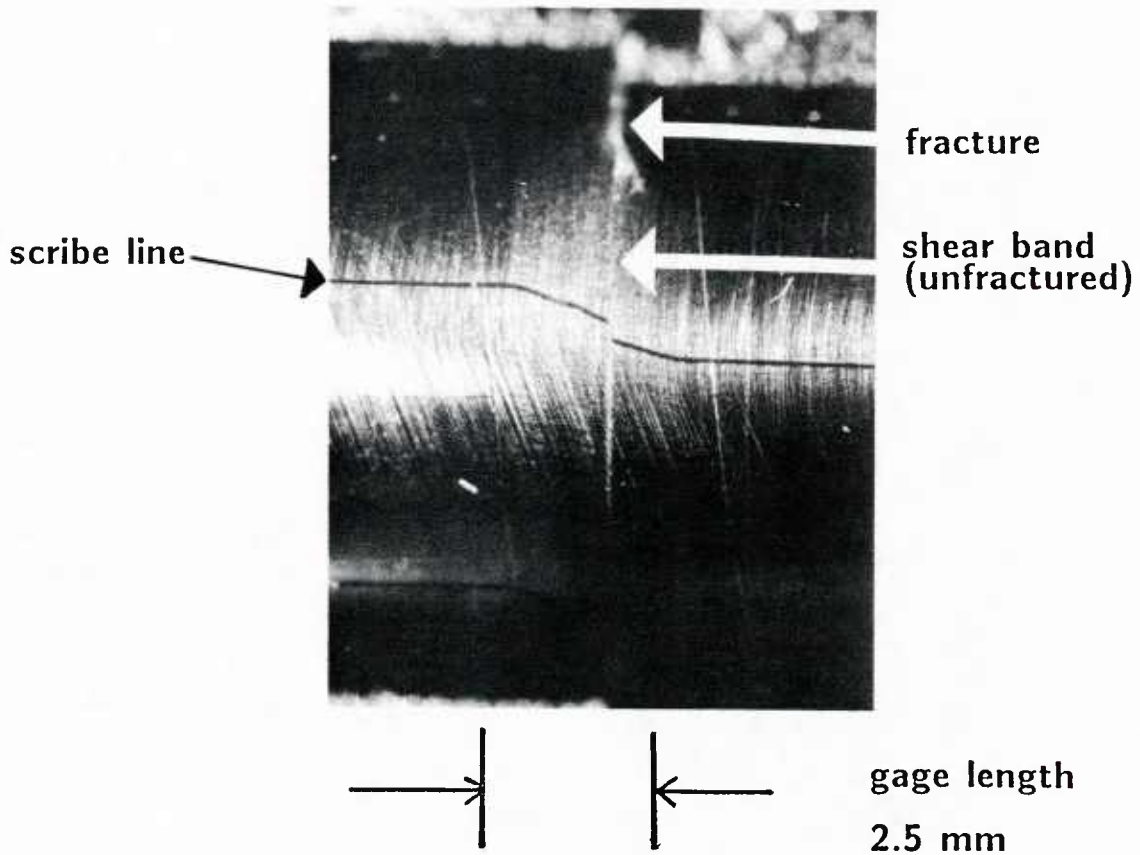
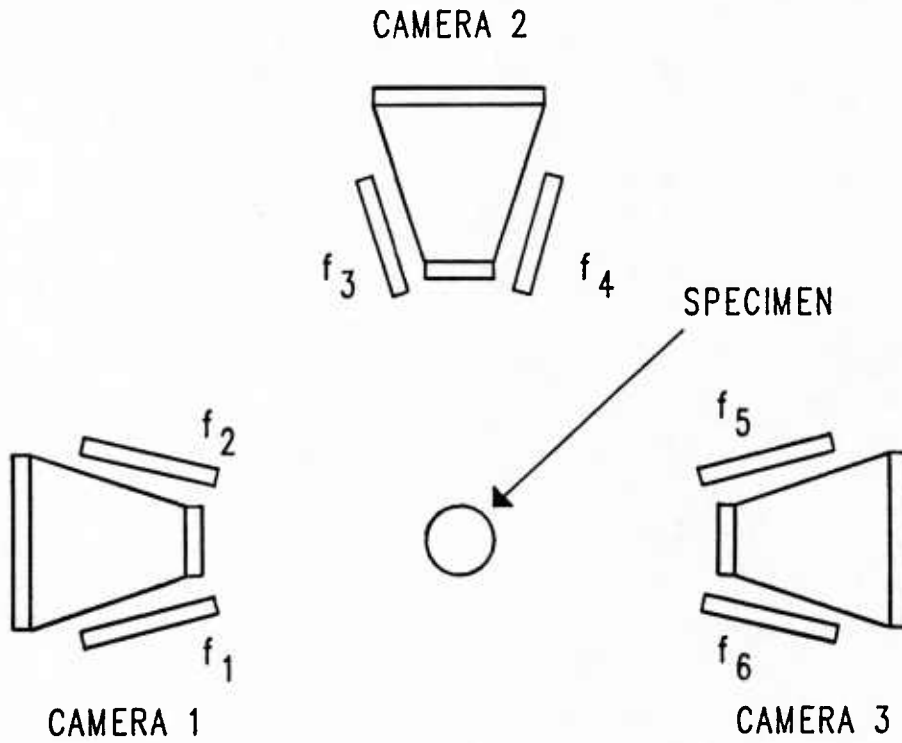


Figure 5: Photograph of a specimen surface after testing showing a shear band and a partial fracture. In this test the nominal strain rate is 1600/s. Within the shear band  $\gamma_{\text{LOC}} = 500\%$ .



EACH FIBER OPTIC TUBE  $f_i$  IS CONNECTED TO A SPARK  
SOURCE OF 2 MICROSECONDS EXPOSURE TIME

Figure 6: Experimental arrangement for taking short-exposure simultaneous photographs of the shear bands.

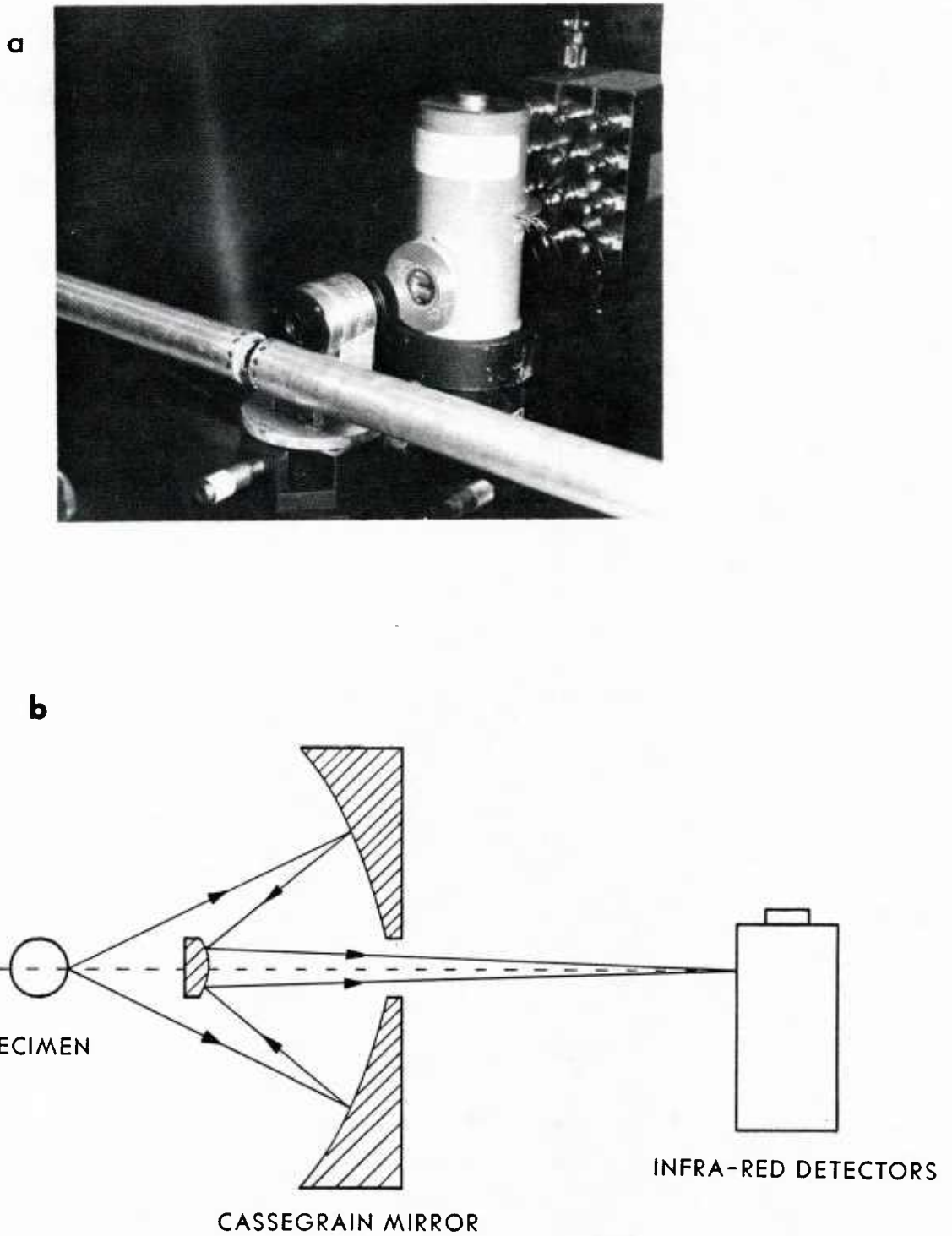


Figure 7: (a) Photograph of InSb detector-mirror system showing I-R detector, Cassegrain mirror and Kolsky bar. Distances are not those used for an actual test. (b) Schematic diagram showing Cassegrain mirror.

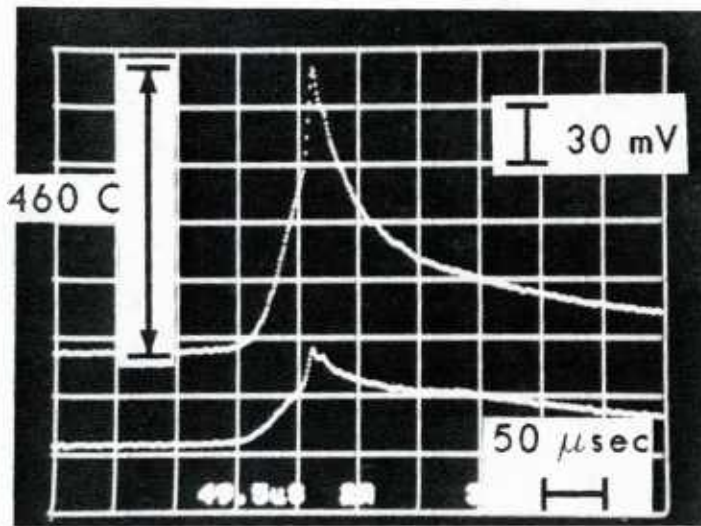


Figure 8: Typical output of two temperature detectors. (Test 13T)

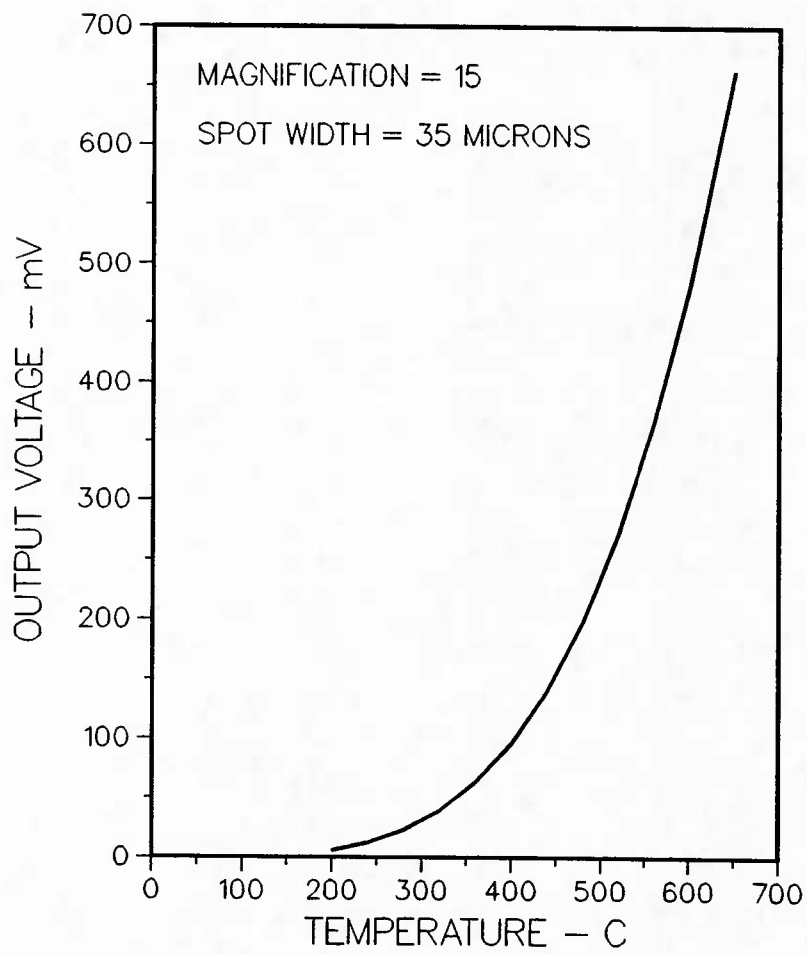


Figure 9: Calibration curve for a spot width of 35 microns.

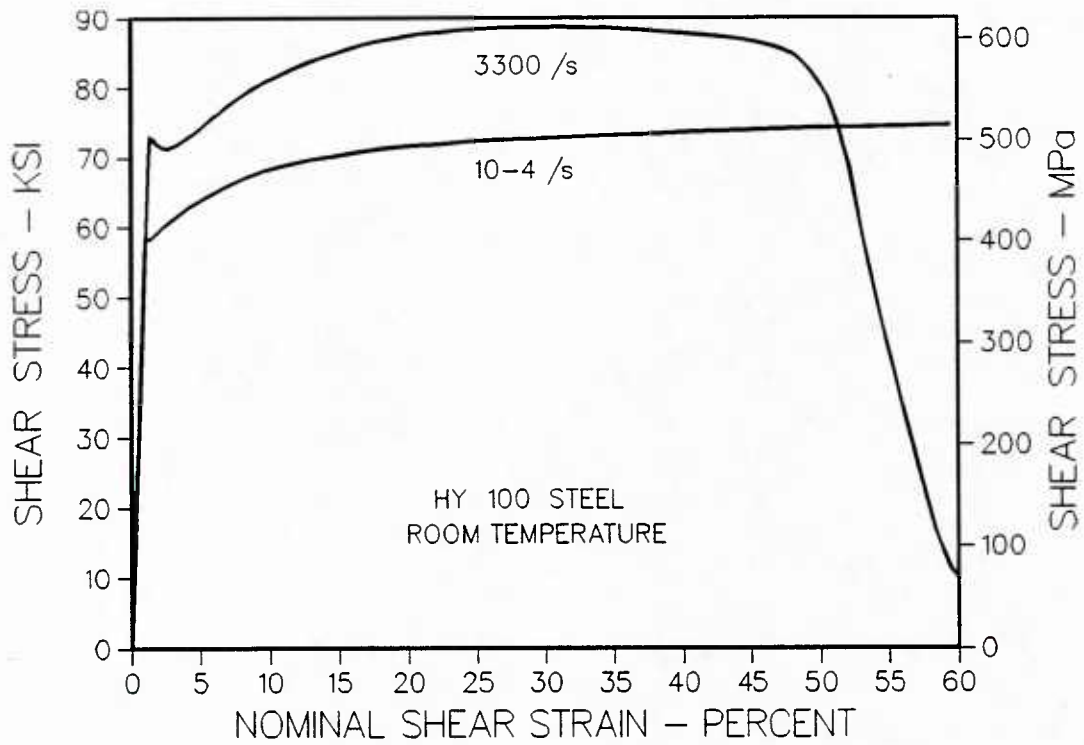


Figure 10: Quasi-static and dynamic stress-strain behavior in shear at room temperature. Fracture in the quasi-static loading occurs at a shear strain of 185%.

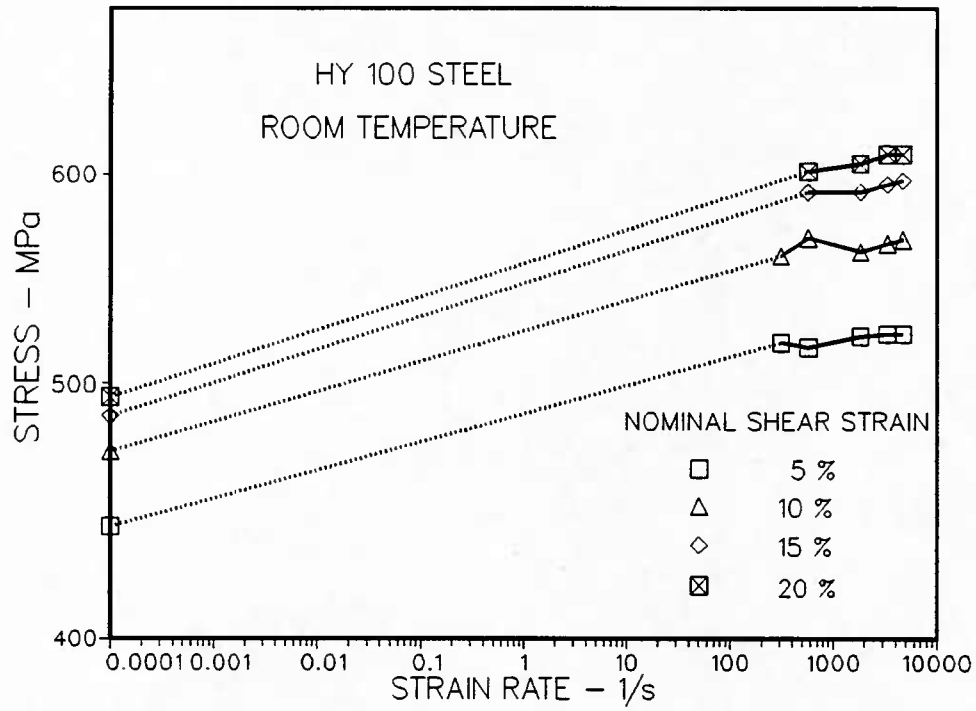


Figure 11: Results of quasi-static and dynamic tests. Shear stress as a function of strain rate for various values of nominal strain.

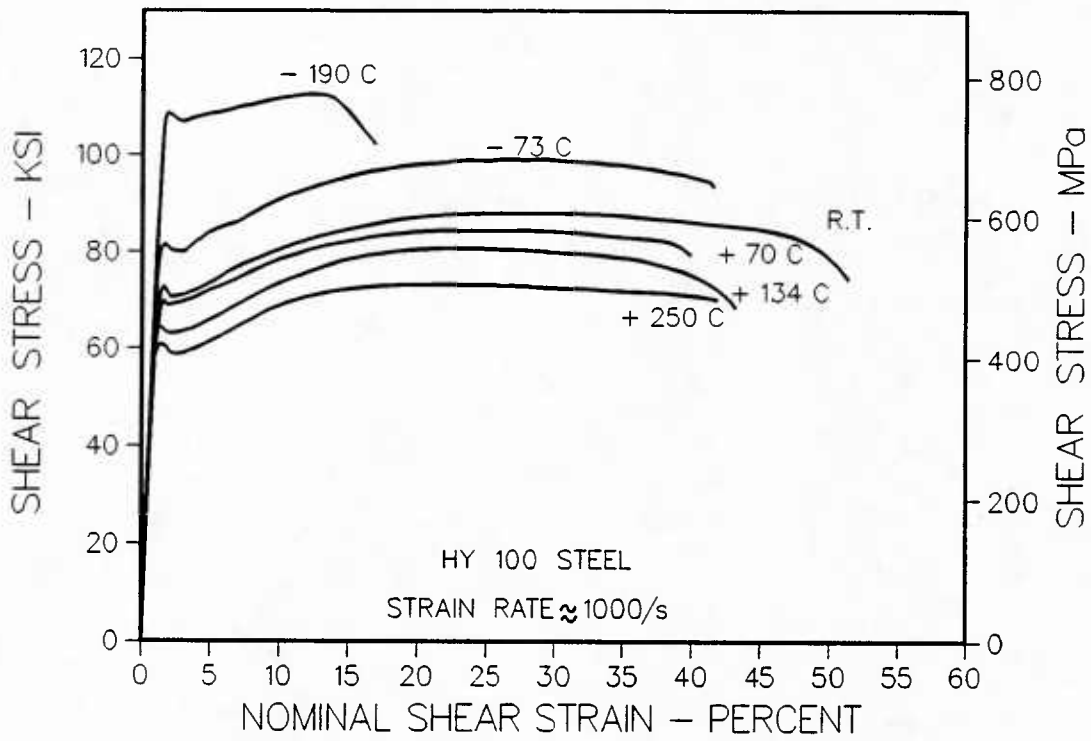


Figure 12: Stress-strain behavior in shear at a nominal strain rate of 1000/s for six different test temperatures.

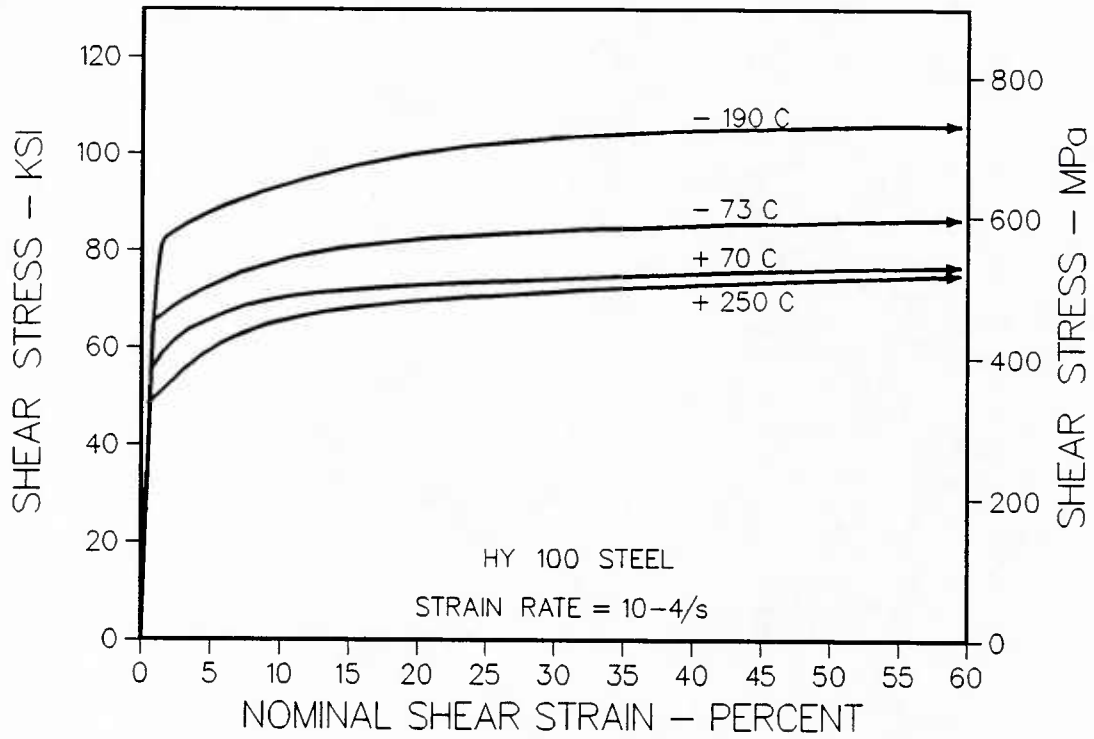


Figure 13: Stress-strain behavior in shear at a nominal strain rate of  $10^{-4}/s$  for four different test temperatures.

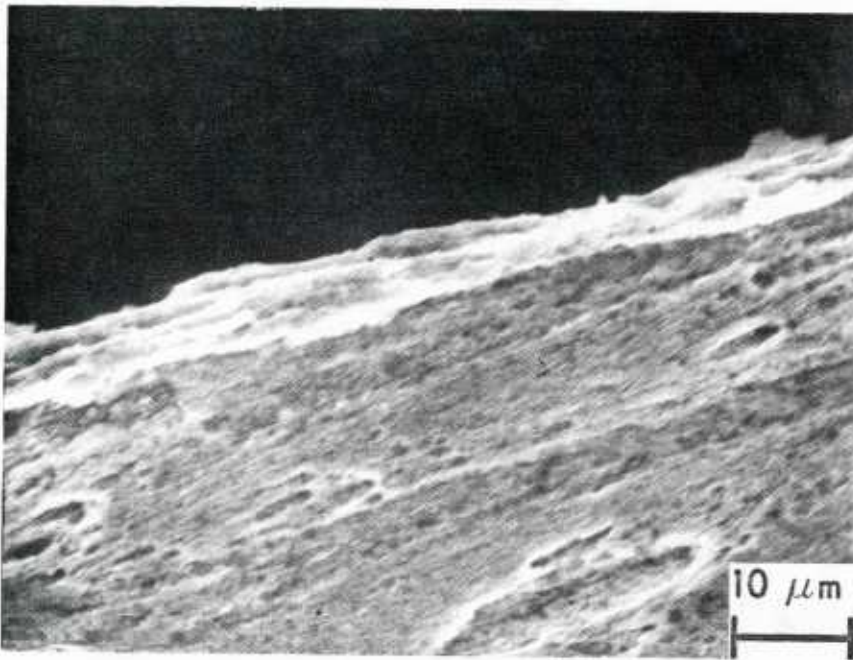


Figure 14: Photograph of the fractured surface of a specimen following dynamic deformation. The surface has been etched with a nital solution resulting in white etched areas.

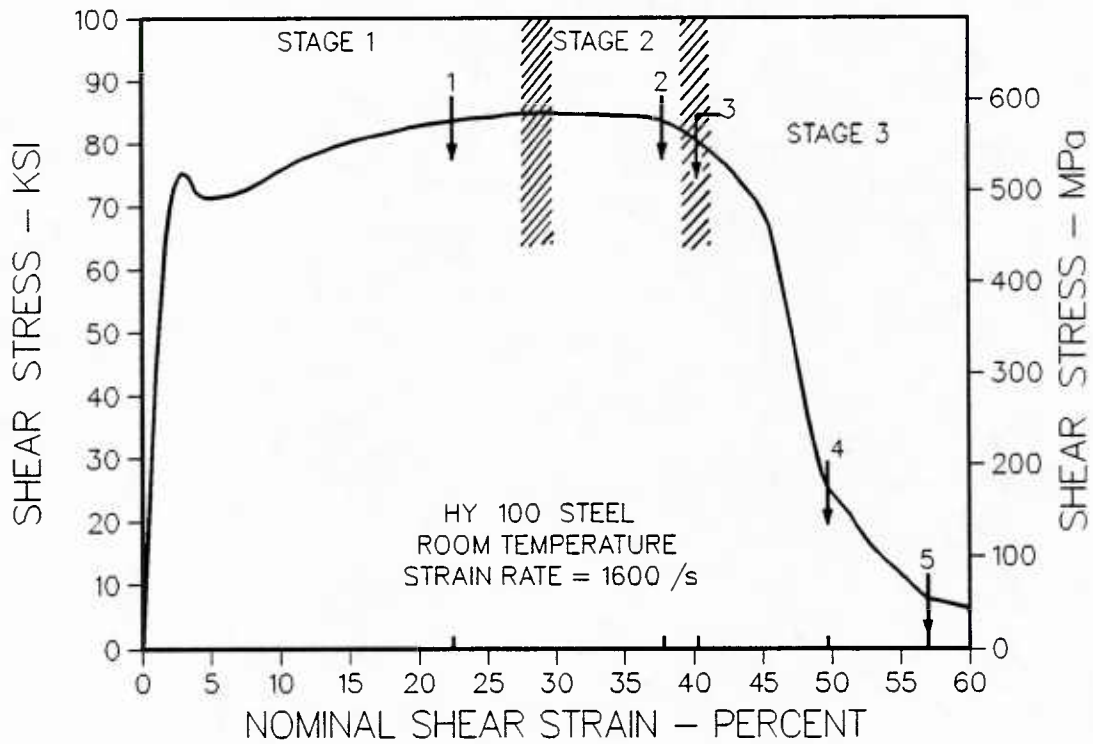
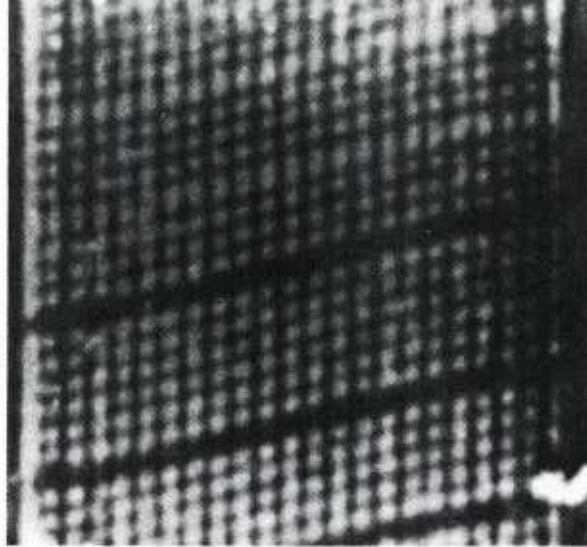
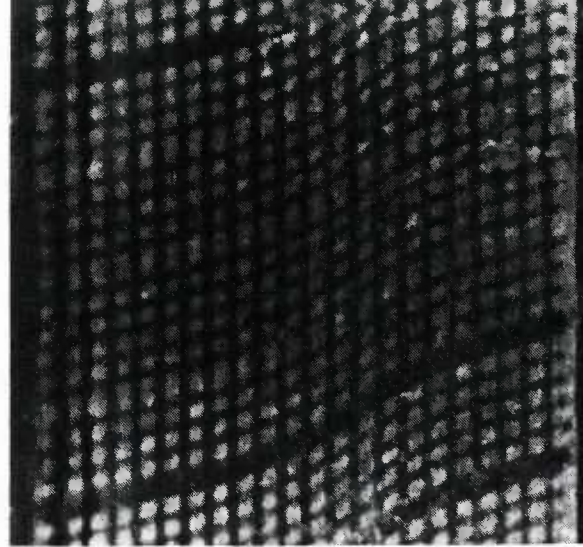


Figure 15: A typical stress-strain curve showing the strain values at which the photographs in Figure 16 are taken.



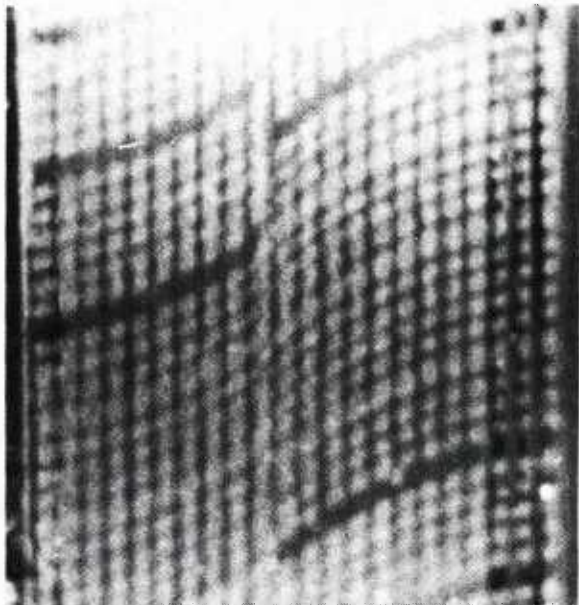
1.  $\gamma_{NOM} = 25\%$



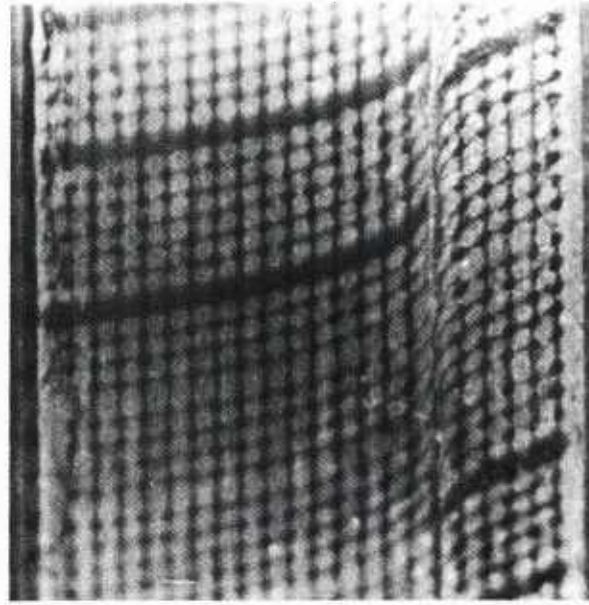
2.  $\gamma_{NOM} = 36\% ; \gamma_{LOC} = 90\%$



3.  $\gamma_{NOM} = 47\% ; \gamma_{LOC} = 350\%$



4.  $\gamma_{NOM} = 55\% ; \gamma_{LOC} = 600\%$



5.  $\gamma_{NOM} = 54\% ; \gamma_{LOC} = 1000\%$

HY-100 Steel

Photographic Records of  
5 Separate Tests

Exposure =  $2\mu\text{sec}$

Scale  $\overline{\hspace{1.5cm}}$  0.5 mm

Figure 16: Photographs of the grid patterns obtained in five separate tests at the nominal strain values shown in Figure 15. The nominal strain rate is 1600/s in each test. Each square in the grid pattern measures 100 microns on a side prior to deformation.

HY-100 Steel - Test 14 -  $\gamma_{\text{NOM}} = 27\%$

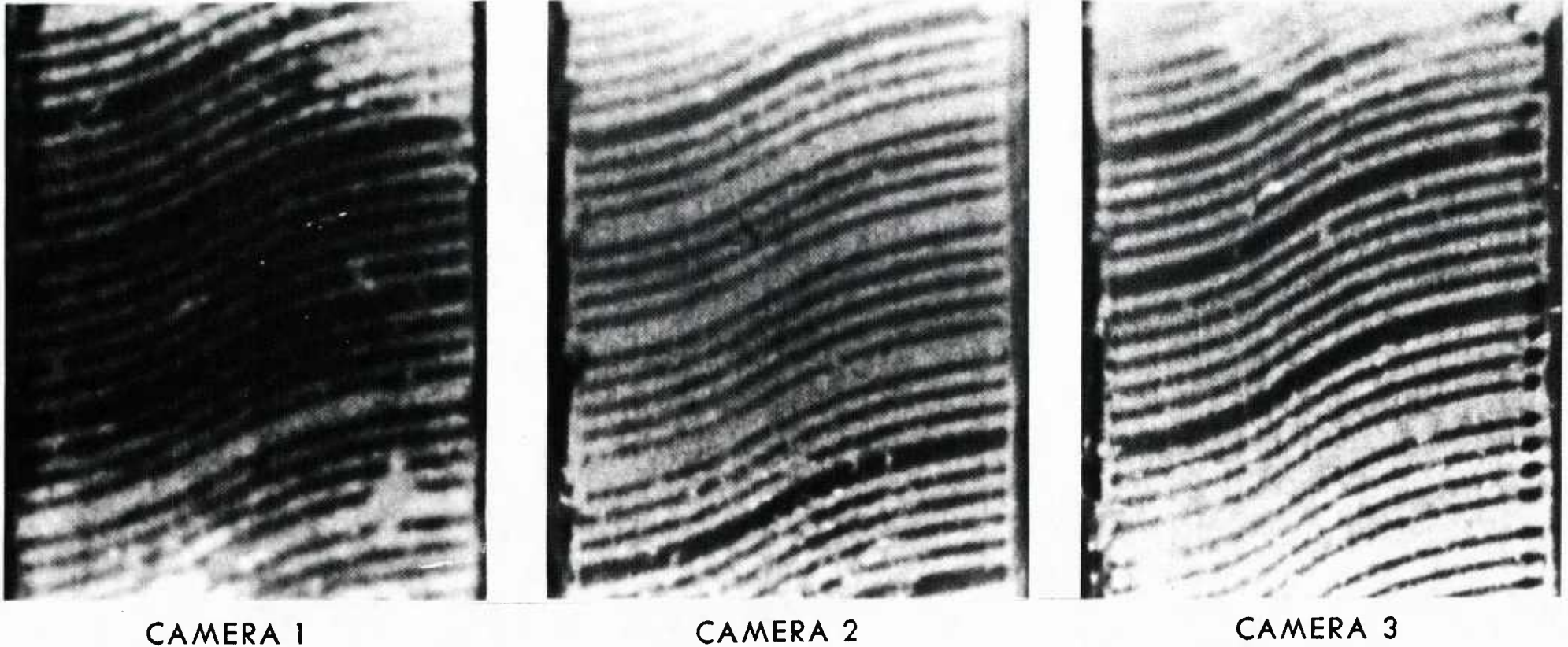


Figure 17: Simultaneous photographs taken at three locations on the same specimen at a nominal strain of 27%, just after the maximum in the stress-strain curve. The exposure time is  $2\ \mu\text{s}$ . Note that the localized deformation is the same at all locations, namely  $\gamma_{\text{LOC}} = 55\%$ . (Test 14 nominal strain rate  $\dot{\gamma} = 1600/\text{s}$ ).

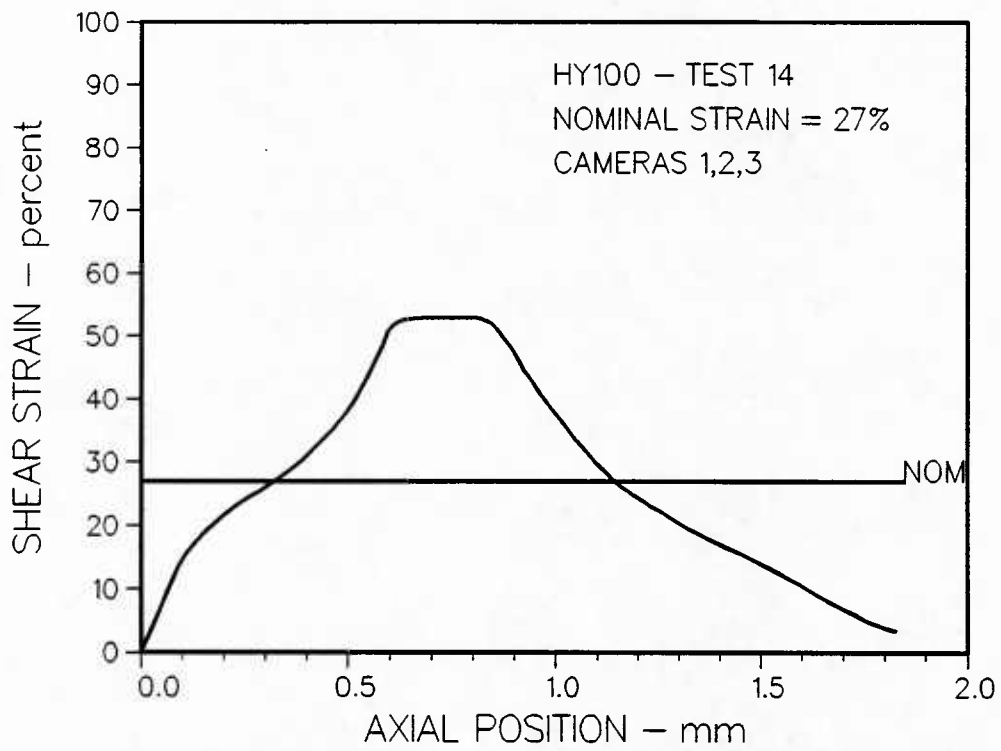
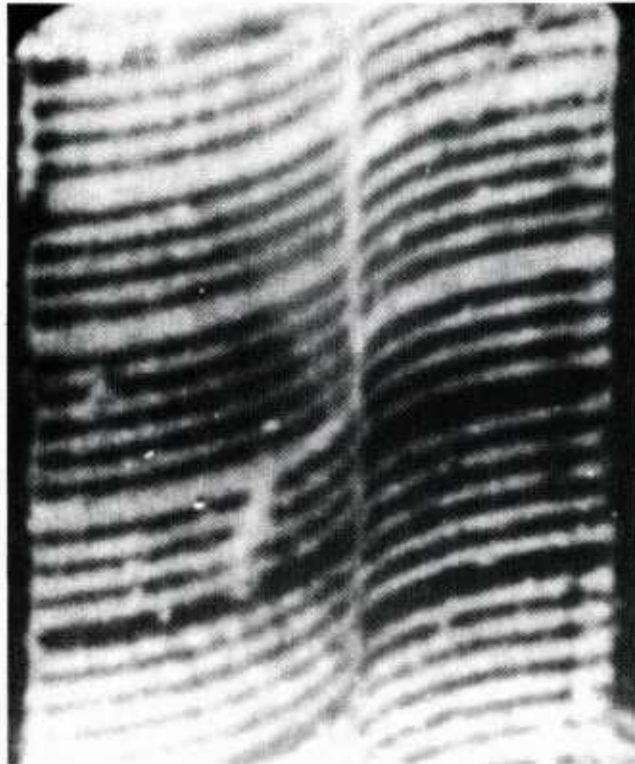


Figure 18: The shear strain distribution at a nominal strain of 27% as obtained from the three photographs in Figure 17.

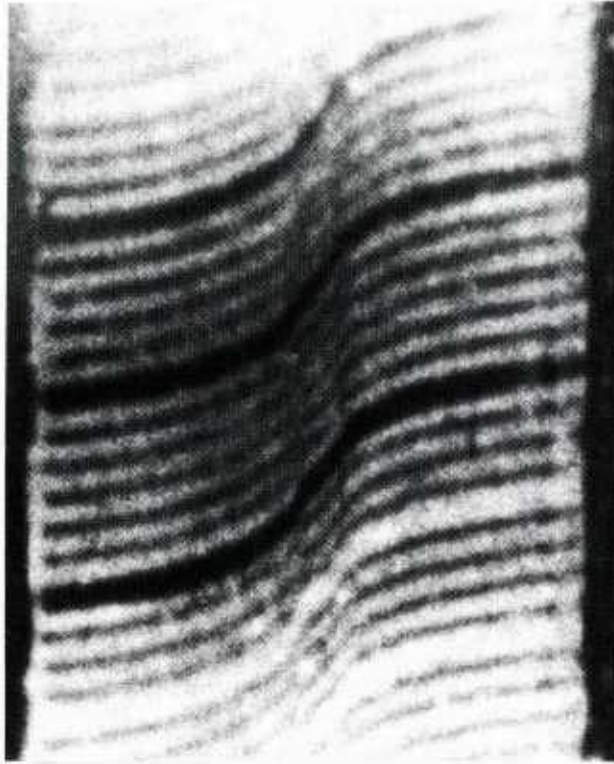
HY-100 Steel - Test 13 -  $\gamma_{\text{NOM}} = 38 \%$



CAMERA 1

$\gamma_{\text{LOC}} = 500 \%$

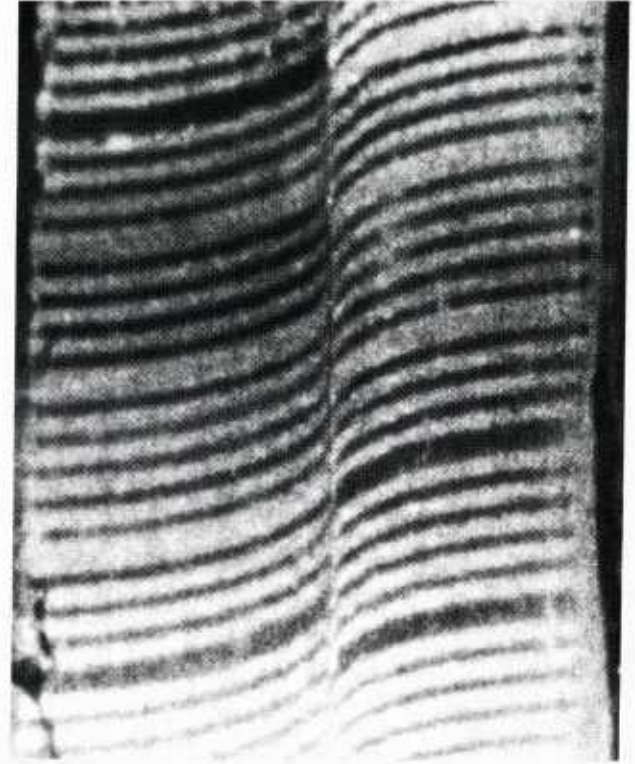
width =  $50 \mu\text{m}$



CAMERA 2

$\gamma_{\text{LOC}} = 130 \%$

width =  $280 \mu\text{m}$



CAMERA 3

$\gamma_{\text{LOC}} = 1900 \%$

width =  $15 \mu\text{m}$

Fracture ?

Figure 19: Simultaneous photographs taken at three locations on the same specimen at a nominal strain of 35%. The maximum in the stress-strain curve occurs at a nominal strain  $\gamma = 21\%$ . The exposure time is  $2 \mu\text{s}$ . Note that the localized deformation is not the same at all locations, as shown in Figure 21. (Test 13, nominal strain rate  $\dot{\gamma} = 1600/\text{s}$ ).

0.5 mm  
|-----|

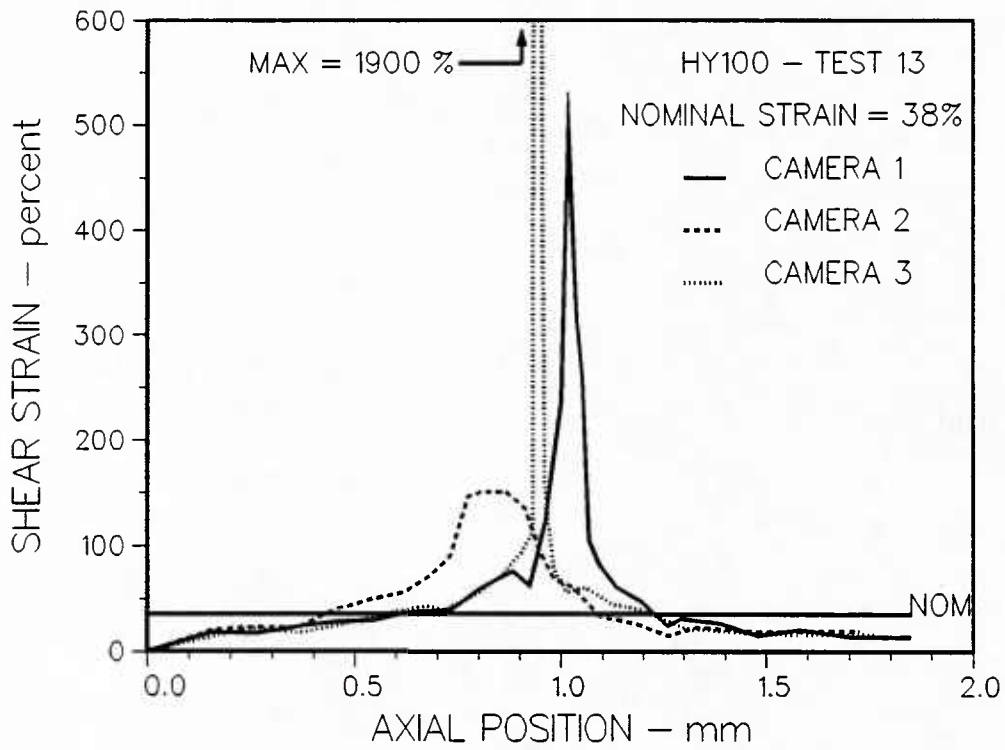


Figure 20: The shear strain distribution at three separate locations on the circumference of the specimen as measured from the simultaneous photographs shown in Figure 19.

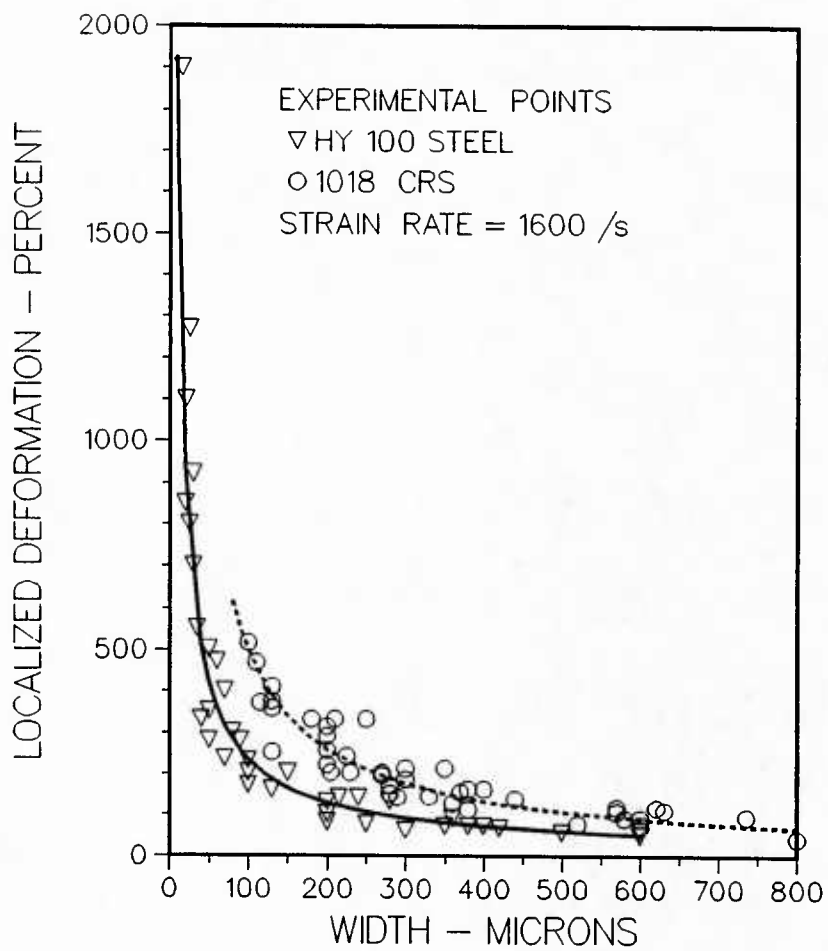


Figure 21: The maximum localized strain as a function of the shear band width in the HY-100 steel and in a 1018 cold-rolled steel. The points represent the results of a number of different tests.



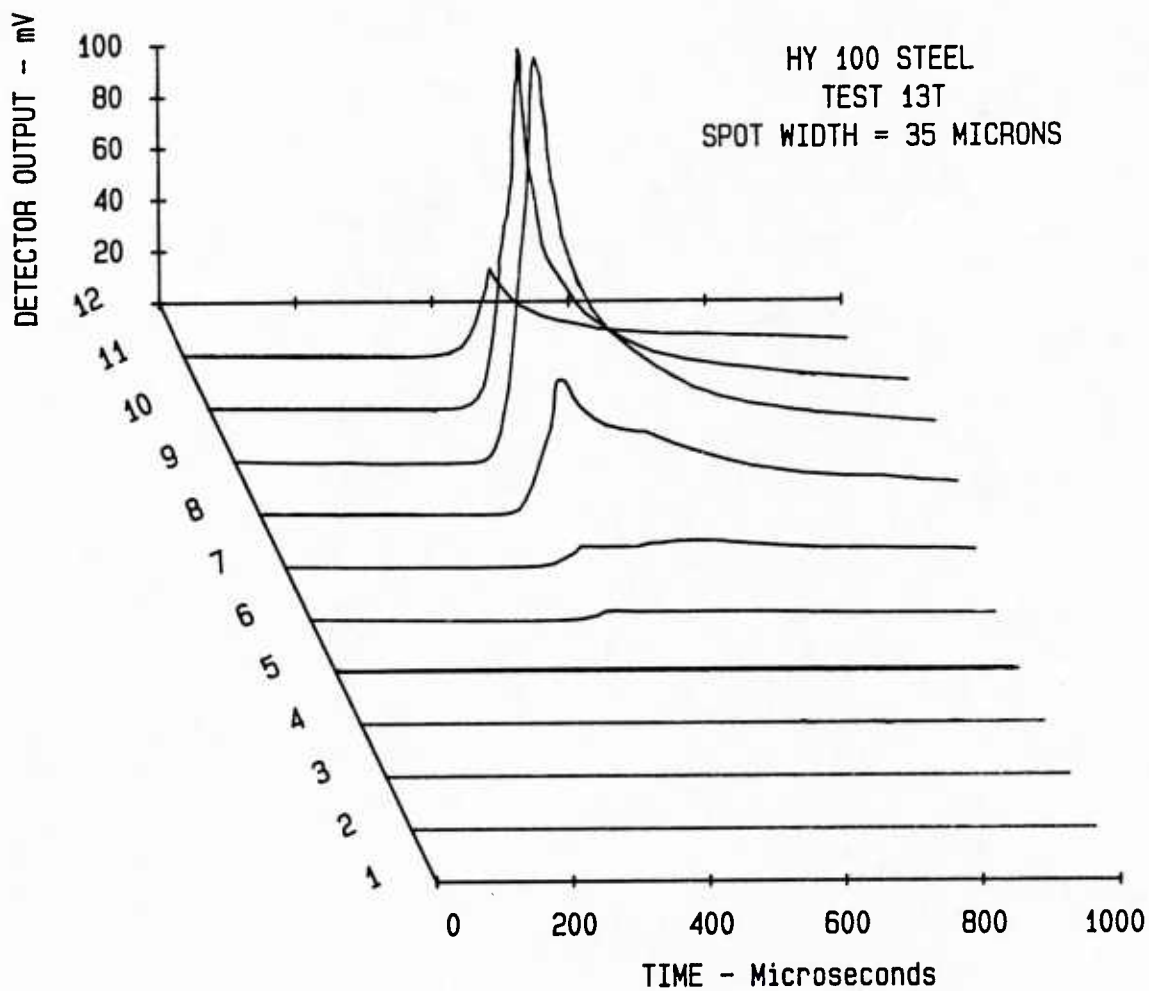


Figure 23: The output of the I-R detectors as a function of time and of axial position in Test 13T. Each spot on the specimen is 35 microns wide and the space between two adjacent spots is 11 microns.

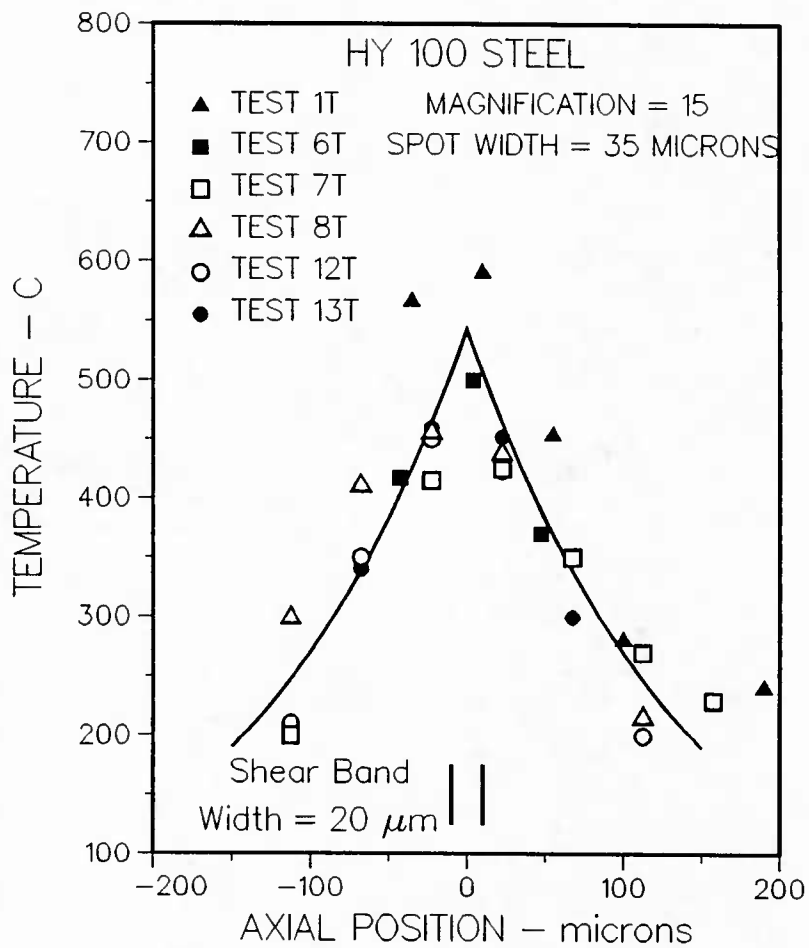


Figure 24: Measured values of the temperature as a function of axial position with respect to the center of the shear band. Note that the width of the observed spot on the specimen (35 microns) exceeds the width of the shear band (20 microns).

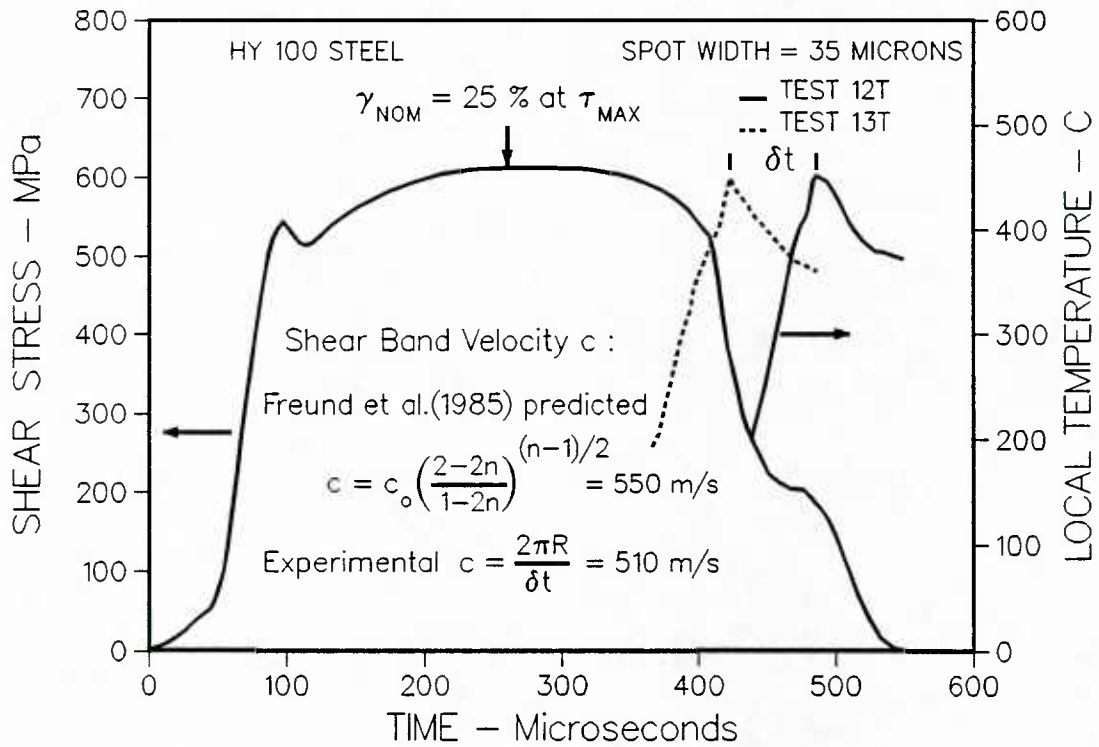


Figure 25: Typical stress-time curve showing the temperature as a function of time in two separate tests. Note that the peak temperatures are separated by about 60 microseconds.